A metabolite binding protein moonlights as a bile-responsive chaperone

Changhan Lee,[1] Patrick Betschinger,[1] Kevin Wu[1], Dawid Zyla[2], Rudi Glockshuber[2] and James C. A. Bardwell[1,3,*]

[1]Department of Molecular, Cellular, and Developmental Biology, and Howard Hughes Medical Institute, University of Michigan, Ann Arbor, MI 48109, USA

[2]Institute of Molecular Biology and Biophysics, ETH Zurich, Switzerland

[3]Lead Contact

*Correspondence: jbardwel@umich.edu

RUNNING TITLE: UgpB is a Bile-Responsive Chaperone

KEYWORDS: chaperone/ protein folding

Word count for abstract: 172

ABSTRACT

Bile salts are secreted into the gastrointestinal tract to aid in the absorption of lipids. In addition, bile salts show potent antimicrobial activity in part by mediating bacterial protein unfolding and aggregation. Here, using a protein folding sensor, we made the surprising discovery that the E. coli periplasmic glycerol-3-phosphate (G3P) binding protein UgpB can serve, in absence of its substrate, as a potent molecular chaperone that exhibits anti-aggregation

activity against bile salt-induced protein aggregation. The substrate G3P, which is known to accumulate in the later compartments of the digestive system, triggers a functional switch between UgpB's activity as a molecular chaperone and its activity as a G3P transporter. A UgpB mutant unable to bind G3P is constitutively active as a chaperone, and its crystal structure shows that it contains a deep surface groove absent in the G3P-bound wild type UgpB. Our work illustrates how evolution may be able to convert threats into signals that first activate and then inactivate a chaperone at the protein level in a manner that bypasses the need for ATP.

INTRODUCTION

Proteins are key catalysts for most cellular processes and maintaining protein stability is an important and regulated process (Balch et al, 2008). When enteric bacteria pass through the gastrointestinal tract, the bacteria encounter various host defense barriers that target protein stability, including gastric acid in the stomach and bile in the duodenum, both of which act to denature proteins (Baba et al, 2006; Cremers et al, 2014). Periplasmic proteins are particularly vulnerable to these environmental denaturants because the outer membrane of the cell allows for the free diffusion of small molecules (Baba et al, 2006). It is known that bacteria have evolved acid-response periplasmic chaperones, HdeA and HdeB, to protect cells from acid-induced protein aggregation in the periplasm (Dahl et al, 2015; Lai et al, 2017; Tapley et al, 2010). However, surprisingly little is known about how bacteria respond to the denaturant properties of bile salts.

Bile salts are amphipathic compounds that not only help in the absorption of lipids in the intestine (Gunn, 2000; Heaton, 1969; Urdaneta & Casadesus, 2017), but also possess potent antimicrobial activity (Urdaneta & Casadesus, 2017), which is elicited by disrupting cell membranes, inducing DNA damage, and causing protein unfolding and aggregation (Cremers et al, 2014; Merritt & Donaldson, 2009; Prieto et al, 2004; Urdaneta & Casadesus, 2017). It is known that bile salts can achieve limited entry into the bacterial cytosol through a flip-flop mechanism (Cabral et al, 1987), and that various chaperones, including Hsp33, DnaK, and GroEL, are upregulated in response to their cytosolic unfolding activity, but it is unclear if or how these chaperones act to protect proteins from the denaturing effects of bile (Bernstein et al, 1999; Cremers et al, 2014; Flahaut et al, 1996; Leverrier et al, 2003; Ruiz et al, 2013). Although

the bacterial periplasm presumably has a much higher exposure to bile salts than the cytosol, remarkably little is known about how periplasmic proteins are protected against bile salts.

Here, we employed high-throughput transposon sequencing (Tn-Seq) combined with a periplasmic protein folding sensor (Foit et al, 2009; van Opijnen et al, 2009), which links protein stability to antibiotic resistance, to screen for host factors that affect periplasmic protein folding. We find that the glycerol-3-phosphate (G3P) binding protein UgpB has a second function, namely moonlighting as a chaperone that appears to be uniquely capable of preventing bile-induced aggregation of a wide variety of proteins present in the periplasm. UgpB alternates between its function as a chaperone and as a G3P binding protein, with its activity being controlled by small molecules known to be present in the intestine. We find UgpB's chaperone activity is inhibited upon binding to its normal substrate G3P, which can be stripped off by pH conditions present in the stomach. A variant of UgpB that fails to bind G3P is constitutively active as a chaperone and newly possesses a binding groove on the surface of its structure deep enough to accommodate peptides. This toggling of UgpB activity by small molecules is consistent with a model in which UgpB acts as a chaperone to guard against bile-mediated aggregation early in digestion and then switches to its role as a G3P binding protein later in digestion, a switch that may be mediated at least in part by rising G3P concentrations caused by digestion.

RESULTS

Use of Tn-Seq and a Protein Folding Sensor in Chaperone Discovery

In efforts to discover previously uncharacterized chaperones in the periplasm of *E. coli*, we combined an *in vivo* selection for improved protein folding with a Tn-Seq approach. Tn-Seq is a high-throughput method that allows one to compare the frequencies of transposon insertion in essentially all genes between two populations, one of which has been subject to a genetic selection (Burby et al, 2017; van Opijnen et al, 2009). Genes that, when disrupted, produce either better or worse growth under the applied selection conditions can thus be identified and subsequently characterized. The selection that we used in this approach is based on the expression of a folding biosensor, whose *in vivo* stabilization is directly linked to increased

antibiotic resistance. This selection, in conjunction with Tn-Seq, provides a facile way of screening the whole genome of *E. coli* for genes that affect the folding of sensor protein. The folding biosensor that we used contains Im7 L53A I54A inserted into a glycine-serine linker between positions 196 and 197 of β-lactamase, a protein that confers ampicillin resistance (Figures 1A and Appendix Figure S1A) (Foit et al, 2009; Quan et al, 2011). Im7 L53A I54A is an unstable and partially unfolded variant of Im7 that mimics the intermediate that accumulates in Im7's folding pathway (Quan et al, 2013). We reasoned that host mutations that stabilize the test protein should increase the ampicillin resistance of strains containing this folding biosensor, whereas those that destabilize the test protein should decrease their ampicillin resistance. Hence in our screen (illustrated in Figure 1A, see Methods for details), we focused in genes that showed an altered transposon insertion frequency after antibiotic resistance selection in strains that contained the tripartite folding sensor relative to a control strain that just contained the intact unfused β-lactamase gene (*bla*). We reasoned that genes that showed an altered insertion frequency in the folding biosensor strain might be involved in folding or stabilizing the biosensor.

Validation of Tn-Seq Use for Chaperone Discovery

In our previous study, we discovered the periplasmic chaperone Spy by isolating mutants that enhanced the stability of Im7 L53A I54A (Quan et al, 2011). As described in figure EV1, we were able to show that the transposon insertion frequencies in *spy* as well as in *baeSR* encoding a transcriptional regulator for Spy are dramatically decreased when cells are subject to ampicillin a selection. Thus we were able to re-isolate Spy mutants by their decreased chaperone activity as well as the transcription factor that controls this chaperone's expression with this Tn-Seq approach. With these results serving as evidence that our genetic strategy is working as intended, we decided to expand our search for genes with altered insertion frequencies in the wild type (WT) strain containing the Im7 L53A I54A tripartite versus one containing the pBR322 control. The lack of expression of Spy in WT strains conveniently allows us to use this genetic approach to search for chaperones or folding factors, in addition to Spy, that affect the stability of Im7.

PstSCA Insertions Answer Selections Conducted in Folding Sensor Containing Strains

To find genes that may contribute to the folding or stability of the test protein Im7, we identified loci that show an altered transposon insertion frequency in the strain encoding the protein folding sensor β-lactamase-Im7 L53A I54A relative to the strain containing the intact β-lactamase encoded by pBR322. Use of the pBR322 control allowed us to exclude genes that contribute to ampicillin resistance for reasons unrelated to the expression, folding, or stability of the test protein. Since both the sensor and the intact β-lactamase genes are under the same transcriptional, translational, and plasmid copy number control, we reasoned that genes affecting these processes will not show a differential insertion frequency between the two strains. Genes involved in ampicillin resistance itself should be disrupted at approximately equal rates in strains containing the intact *bla* gene versus tripartite fusions derived from the *bla* gene.

One locus that showed a highly elevated transposon insertion frequency in the biosensor strain relative to the control encoded the *pstSCA* genes (Figure 1B). *PstSCA* encodes an ATP-binding cassette (ABC) transporter for phosphate uptake (Gardner et al, 2015). To confirm that insertions within *pstSCA* genes were able to specifically enhance ampicillin resistance of strains containing the Im7 folding biosensor, we transduced deletion mutants of the individual *pst* genes into the biosensor strains and into control strains containing only the intact β-lactamase gene, and then tested for ampicillin resistance (Figure 2A). Deletions of, or insertions into the *pstS*, *pstC*, or *pstA* genes substantially increased ampicillin resistance in the presence of β-lactamase-Im7 L53A I54A, but did not enhance resistance of strains containing intact β-lactamase or β-lactamase-linker constructs (Figure 2A, Appendix Figures S1A, and S2). These results suggested that the *pstSCA* genes were good candidates for genes involved either directly or indirectly in the stability of the protein folding biosensor and thus were worthy of further analysis.

PstSCA Mutants Result in Increased Levels of the Protein Folding Sensor *In Vivo*

As measured by Western blotting, the protein level of the Im7 folding biosensor is ~14-fold lower than levels of intact β-lactamase found in WT strains. As we found previously (Quan et al, 2011), this is presumably again due to protein instability conferred by the Im7 portion of this folding biosensor. Tn5 insertions in the *pstS*, *pstC*, or *pstA* genes resulted in a 2- to 4-fold increase in the levels of the β-lactamase-Im7 L53A I54A folding biosensor, but no change in the levels of intact β-lactamase (Figure 2B). Moreover, the β-lactamase activity contained in

periplasmic cell extracts from cells expressing the folding biosensor was 4- to 5-fold higher in the *pstS*, *pstC*, or *pstA* mutants than it was in strains that are WT for the *pst* locus (Figure 2C). These results suggested that we may have indeed identified genes involved in determining the stability and or expression of the folding biosensor.

To test if the effect of the *pst* mutants on the folding biosensor extended to the Im7 protein itself, we expressed Im7 and Im7 L53AI54A proteins on their own, in the absence of the fusion context. Enhancement of Im7 L53A I54A levels was observed in the *pstS* and *pstA* mutant strains was indeed observed (Figures 2D and S3). WT Im7, which is well folded and stable compared to the Im7 L53A I54A variant, was expressed at a very similar level in WT and *pstS* mutant strains (Appendix Figure S3). This is consistent with our observation that *pst* mutants do not significantly enhance ampicillin resistance in the presence of β-lactamase-Im7 (Appendix Figures S2A and 3A). These results provided a preliminary indication that the *pstSCA* mutations are able to stabilize Im7 L53A I54A *in vivo*.

UgpB Acts to Enhance the Protein Level of Im7 L53A I54A

Our studies showed that mutants lacking components of the *Pst* machinery accumulate higher levels of folded Im7 L53A I54A than wild-type *E. coli* strains. Since it is known that disruption of *pst* genes substantially affects the expression of a number of diverse genes (Crepin et al, 2008), we wondered whether the observed effects were a direct or indirect effect on protein expression, folding and/or stability. We therefore considered the possibility that *pst* disruption increases the expression of some other proteins that then more directly act to stabilize the protein folding sensor. To investigate this, we performed liquid chromatography-mass spectrometry to quantify the levels of proteins present in whole cell lysates of strains containing *pst* disruptions. As previously observed (Crepin et al, 2008), a wide variety of phosphate transportation-related proteins were overexpressed in *pst* mutant strains (Dataset EV1). We selected six of these overexpressed proteins as candidates (PhoA, PhoE, PhnD, UgpB, DsbC, and FkpA) based on two criteria: i) periplasmic localization, since β-lactamase is expressed and active in the periplasm and ii) expression levels, since proteins can be stabilized by chaperone overexpression or protease depletion. Given our interest in chaperone discovery, we selected proteins that are present at higher levels (>2-fold) in the *pst* mutants as compared to WT strains.

To test if the overabundance of these candidate proteins was directly responsible for the apparent stabilization of the Im7 L53A I54A folding sensor in a *pst* deletion background, we co-deleted them from a *pstS* null strain and determined if the ampicillin phenotype linked to the stabilization of the biosensor simultaneously disappeared. We found that additional deletion of p*hoA*, *phoE*, *phnD*, *dsbC*, or *fkpA* deletions had no effect on the ampicillin resistance encoded by the Im7 L53A I54A folding biosensor (Appendix Figure S4), implying that these 5 genes were not responsible for the accumulation of Im7 observed in *pst* mutants. However, introducing a *ugpB* deletion into a *pstS* or *pstA* null mutant made these cells just as ampicillin sensitive as did a *pstS*+ or *pstA*+ strain background (Figure 3A, Appendix Figures S4 and S5). *UgpB* deletions in the *pst* null mutant specifically affected the ampicillin resistance of the destabilized β-lactamase-Im7 L53A I54A folding biosensor, but did not affect the ampicillin resistance of any of the other β-lactamase constructs, β-lactamase itself, β-lactamase containing a 33 amino acid glycine-serine linker, or β-lactamase-Im7, all which encode more stable proteins (Figure 3A and Appendix Figure S5). Taken together, these observations indicate that the UgpB overexpression induced by the *pst* deletion is most likely directly responsible for specifically enhancing ampicillin resistance through its ability to stabilize the Im7 L53A I54A protein folding sensor.

These observations are surprising, as UgpB's only known activity to date is its ability to function as a periplasmic Glycerol-3-Phosphate (G3P) binding protein that functions in G3P transport (Wuttge et al, 2012). Chaperones tend to be very abundant proteins (Yan et al, 2019), so it is interesting to note that based on our proteome analysis in the *pstS* or *pstA* mutants, UgpB was induced >16-fold (Dataset EV1), to very high levels, similar to levels of UgpB overexpression that had been previously reported in *pst* mutant strains (Crepin et al, 2008). This level of overexpression makes UgpB the most abundant protein present in periplasmic extracts of *pstS* or *pstA* mutants, (Figure 2D, Appendix Figures S3, and S6). To test whether overexpression of UgpB is sufficient to enhance β-lactamase-Im7 L53A I54A levels, we expressed UgpB from an arabinose-inducible promoter in a *ugpB* deletion mutant. We found that this overexpression confers as high a level of ampicillin resistance as is present in *pst* mutations, implying that UgpB overexpression is responsible for the enhanced ampicillin resistance seen in the *pst* mutations (Figure 3B). Overexpression of UgpB also leads to accumulation of Im7 L53A I54A itself, independent of it being present in a fusion context (Figure 3C). We conclude that UgpB overexpression is sufficient to cause *in vivo* accumulation of stably folded Im7 L53A I54A.

UgpB Prevents Bile Salt-Induced Protein Aggregation

To analyze whether UgpB has a general chaperone activity, we tested its influence on classic chaperone substrates using light scattering measurements. We found that UgpB does not interfere with the heat-induced aggregation of the classic chaperone substrates malate dehydrogenase (MDH), citrate synthase (CS), or luciferase. These results make physiological sense since periplasmic proteins tend to be very thermostable, likely eliminating the need for chaperones to protect them from heat-induced aggregation. In searching for a possibly more physiologically relevant stressor, we noted that UgpB expression is highly induced upon bile stress in *Salmonella enterica*, and that a *ugpB* deletion mutant of *E. coli* shows high sensitivity to bile salts (Hernandez et al, 2012; Nichols et al, 2011). Bile salts are amphipathic compounds that help in the absorption of lipids in the intestine (Urdaneta & Casadesus, 2017). They are also well known for their antimicrobial activity and are particularly potent against Gram-positive bacteria (Urdaneta & Casadesus, 2017). Although not as well publicized, bile salts also act as detergents, causing protein unfolding and aggregation (Cremers et al, 2014). We confirmed that the disruption of *ugpB* in the *E. coli* BL21(DE3) strain slightly increases the susceptibility of the mutant to bile salts, and demonstrated that the overexpression of UgpB from the pTrc99a plasmid under the IPTG-inducible promoter confers a significantly increased resistance to cholate (CHO), the most prevalent primary bile salt in the human intestine, particularly at elevated temperatures (Figure 4A). Since bile salts directly unfold and aggregate proteins (Cremers et al, 2014; Urdaneta & Casadesus, 2017), we examined whether UgpB can prevent bile salt-induced protein aggregation *in vitro*. We used MDH, lactate dehydrogenase (LDH), and CS as model substrates and induced their aggregation by treatment with CHO. We monitored protein aggregation by light scattering or analyzing protein solubility (Figures 4B and 4C; Methods). Addition of CHO induces the aggregation of MDH, LDH, and CS (Figures 4B, 4C, EV2, and Appendix Figure S10). Notably, UgpB efficiently prevents CHO-induced aggregation of all three of these proteins in a dose-dependent manner. UgpB also shows potent anti-aggregation activity toward the CHO-induced aggregation of total *E. coli* lysates (Figure 4F). Our results suggest that UgpB does function as a molecular chaperone, with a surprisingly broad substrate spectrum, that is capable of preventing bile salt-induced protein aggregation.

Since chaperones often exhibit functional redundancy, we decided to investigate whether other periplasmic chaperones also display anti-aggregation activity in response to CHO-induced

protein aggregation. Spy, SurA, and OsmY are known periplasmic chaperones (Ruiz et al, 2013; Stull et al, 2018). SurA is involved in maintaining the solubility of outer membrane proteins while they are in transit through the periplasmic space (Stull et al, 2018). Spy is a stress-inducible chaperone that prevents stress-induced protein aggregation and assists in the folding of its clients (Quan et al, 2011). OsmY exhibits anti-aggregation activity and is induced by bile salt treatment (Hernandez et al, 2012; Lennon et al, 2015). These other chaperones are inactive in preventing CHO-induced protein aggregation using the model substrate MDH, at least under the conditions tested (Figure 4D), providing evidence that UgpB's anti-aggregation activity in response to bile salt stress is unique.

The Anti-Aggregation Activity of UgpB Is Regulated by Binding to G3P

Since UgpB can be present as either G3P-free apo or G3P-bound holo forms depending on the environmental conditions to which cells are exposed, we compared the chaperone activity of G3P-bound form (hereafter referred to as $UgpB_{G3P}$) and G3P free UgpB. We found that the anti-aggregation activity of UgpB is strongly modulated by the presence G3P. After expression of UgpB in the cytoplasm and subsequent purification, UgpB is almost entirely G3P bound. The observed G3P occupancy is 90% likely because G3P, as a key glycolysis intermediate (Appendix Figures S7-9) is abundant in cytoplasm (Lemieux et al, 2004). These G3P-bound UgpB preparations show roughly 10-fold lower anti-aggregation activities than G3P free UgpB that has had its G3P stripped off by dialysis performed in the presence of denaturant followed by protein refolding (Figure EV2). In agreement with this, addition of G3P inhibits UgpB's chaperone function (Figures 4E, 4F, and Appendix Figure S10). UgpB is present in the periplasm of bacteria, for its chaperone activity to make physiological sense and for the genetic selection for chaperone activity to have succeeded, periplasmic UgpB should be at least partially G3P free. UgpB in periplasmic extracts was determined by absorption experiments to have only 36% G3P occupancy (Appendix Figure S9E). Since some G3P may be released from the cytosol during the periplasmic extraction procedure, this likely represents the upper limit for G3P occupancy in the periplasm *in vivo*. These results suggest that the active chaperone form of UgpB is present *in vivo* and is thus likely involved in the stabilization of protein folding sensor.

To obtain additional evidence that release of G3P activates the chaperone activity of UgpB, we tested the chaperone activity of two variants (W169S and W169S/W172S), which are

known to be defective in binding G3P (Wuttge et al, 2012). If activation of chaperone activity is due to G3P release, we reasoned that these variants should be constitutively chaperone active, independently of the presence or absence of G3P. Indeed, we observed that G3P did not diminish the anti-aggregation activity of both of these G3P defective variants, while the activity of wild type UgpB is completely abolished in the presence of G3P (Figures 4G, 4H). Notably, both variants exhibit lower anti-aggregation activity than does the wild type UgpB, suggesting that the tryptophan residues W169 and W172 are involved not only in G3P binding but also in the anti-aggregation activity of UgpB.

The substitution of the two tryptophan residues likely affects the chaperone activity of UgpB in two ways, first by making UgpB constitutively chaperone active because these tryptophan residues are involved in G3P binding but second since these hydrophobic residues are also likely to be involved in peptide binding, these substitutions are also likely to decrease the chaperone activity. To distinguish between these effects, we attempted to isolate the UgpB variants that are only defective in G3P binding and are not likely to be directly involved in peptide binding. We selected glutamate 66 and arginine 374 and substituted them with alanine and valine, respectively. These two residues contain charged side chains that are directly involved in G3P binding (Fenn et al, 2019; Wuttge et al, 2012). We found that the E66A and R374V variants of UgpB exhibit the same of chaperone activity as does the G3P-free form of wildtype UgpB i.e they are constitutively chaperone active (Figures 4I, 4J). Importantly, in contrast to wildtype UgpB, the chaperone activity of these UgpB variants is not negatively affected in the presence of G3P (Figures 4I, 4J). These constitutively chaperone active mutants strongly support our hypothesis that G3P binding is a switch that modulates the chaperone activity of UgpB.

Release of G3P opens up a deep groove on the surface of UpgB's structure

To gain more structural insights into the mechanism of G3P-regulated UgpB's chaperone activity, we decided to crystallize and determine the structure of chaperone active, G3P free UgpB. We were unsuccessful in crystalizing apo WT UgpB, possibly because the process of stripping G3P involves denaturation and refolding which may interfere with crystallization. However, attempts to crystallize a G3P-binding defective variant (W169S/W172S) were successful and we solved its structure to 1.25 Å resolution (Appendix Table S3). The overall

structure of this UgpB variant adopts a more open conformation than the G3P-bound structure does, very similar to what is known about the differences in structure between apo and holo UgpB from *Mycobacterium tuberculosis* (Fenn et al, 2019) (Appendix Figure S11). Since the W169S/W172S variant of *E. coli* UgpB shows no detectable ability to bind G3P (Wuttge et al, 2012), we reasoned that its crystal structure should mimic the conformation of apo WT UgpB. To even better mimic ligand-free wild-type UgpB, we constructed a structure model using the SWISS-MODEL program of the wild type UgpB structure by reverting the W169S/W172S mutations to their native tryptophans. While some local regions, including residues 168-174 in the modeled structure are slightly shifted towards the domain interface relative to the ones in the W169S/W172S mutant crystal structure, the overall conformation of modeled structure is nearly identical to the crystal structure of the mutant with an r.m.s.d. of 0.579 Å (Appendix Figure S12). We then used the modeled structure of apo WT UgpB for the further structural analysis and comparison.

Upon binding of G3P, UgpB's conformation is locked in a closed form via extensive interactions between G3P and both domains of UgpB including residues E66,W169, W172 and R374 (Wuttge et al, 2012); in the absence of G3P, the structures of individual domains are very similar to those found in the G3P-bound form (Appendix Figure S13A), while the overall structure of UgpB undergoes the repositioning of the N and C terminal domains via rotation of a domain relative to the other by ~21° (Figure 5A and Appendix Figure S13B). Most interestingly from the perspective of chaperone activation, a deep continuous groove with a solvent-accessible volume of 940 $Å^3$ at the domain interface is exposed to the solvent in the apo form (Figure 5B). This groove, which is closed in the holo form, exposes a number of hydrophobic residues (Met10, Leu14, Tyr42, Tyr65, Val67, Trp169, Trp172, Ala 246, G249, Ala252, Gly 283, Gly284, Tyr 323 and Pro371), most notably Trp169 and Trp172. These two tryptophan residues when replaced by Ser result in no G3P binding (Wuttge et al, 2012) and constitutive but lower chaperone activity (Figure 4G, 4H). In addition to hydrophobic residues, the groove comprises some polar residues (Ser9, Ser121, Thr233, Ser247, Ser250 and Thr321) and a few charged residues (Glu66 and Arg374) (Figure 5B). Notably, many of these solvent-exposed residues, including Tyr42, Glu66, Ser121, Trp169, Trp172, Gly284, Tyr323 and Arg374, directly associate with G3P in the closed form (Wuttge et al, 2012). To further examine if this solvent-exposed groove is of sufficient size to accommodate polypeptide segments, we performed

computational docking using the MDockPrp server (Xu et al, 2018). We attempted to dock a set of 24 different MDH peptides onto the structure of apo UgpB. Strikingly, for all the tested peptides the lowest energy docking score was into the groove (Figure EV3). Moreover, among the top 10 predicted models for all peptides, 229/240 (95%) of the docking results show the peptides docked into the same groove. In contrast, when we attempted to dock the peptides onto the holo UgpB structure, the best docking energy scores placed the peptides at various places around the surface of UgpB (Figure EV3B) and the docking energies were all higher than docking onto the apo UgpB wild type structural model (Dataset EV2). Our structural analysis and docking simulation suggest that the continuous groove between the two domains in the apo UgpB structure may comprise at least part of a putative binding site for unfolded substrates.

Transition from Acidic to Neutral pH Strips G3P and Activates UgpB's Chaperone Activity

Our results suggest that UgpB only exhibits chaperone activity against bile salt induced protein unfolding when UgpB is G3P-free. We wondered how this requirement might possibly be linked to bile salt expose, which most commonly takes place in the small intestine of mammals. We know that when bacteria pass through the stomach, they are exposed to an acidic environment (pH 1–3). Since acidic conditions unfold proteins, including UgpB (Figure 6A) (Goto et al, 1990), we hypothesized that passage through the stomach might strip G3P from UgpB and hence activate its chaperone activity. To test what will likely happen to UgpB upon exposure of bacteria to stomach acid followed by their transition to the pH neutral duodenum, we exposed $UgpB_{G3P}$ to pH 2 for 20 min and subsequently shifted the protein to pH 7 (see Methods). We then determined the G3P content of the UgpB by adding G3P and following tryptophan fluorescence (Figure 6B). Using this assay, we determined that UgpB indeed loses its bound G3P following acid-mediated denaturation. Consistently, we observed that the chaperone activity of UgpB is activated by the transition from pH 2 to 7, and that the addition of G3P can again inactivate the chaperone function of UgpB (Figure 6C). We then examined whether G3P can compete for client binding to UgpB. We found that addition of G3P enhances the aggregation of CHO-induced MDH in a dose-dependent manner (Figures 6D, EV2). These results strongly suggest that G3P can compete with client proteins for UgpB's binding, suggesting that UgpB's G3P binding and chaperone activities are likely mutually exclusive activities.

DISCUSSION

To gain access to the intestinal tract, enteric bacteria, such as *E. coli*, must survive both the highly acidic environment of the stomach and also must be resistant to high levels of bile salts to which they are exposed to in the duodenum. These conditions present challenges both to bacterial proteins and to the chaperones that are there to protect them. Periplasmic proteins are particularly vulnerable to these changing conditions because the outer membrane contains pores, leaving the periplasm essentially unbuffered and vulnerable to molecules smaller than ~600 Da, including protons and bile salts, both of which are effective protein denaturing agents (Baba et al, 2006; Cremers et al, 2014; Lai et al, 2017). Increasing the challenge to periplasmic chaperones is the complete lack of ATP in this compartment; ATP is a cofactor that plays a key role in modulating the activity and substrate binding affinity of many chaperones (Hartl et al, 2011; Midgett et al, 2017; Olive et al, 2007). The absence of ATP in the periplasm has forced evolution to come up with alternative mechanisms that periplasmic chaperones use to govern their activity. One periplasmic chaperone, HdeA, is activated by acid both transcriptionally and directly at the protein level. Low pH acts to partially unfold and activate HdeA, which then tightly binds its substrates, preventing their aggregation. Neutralization is followed by substrate release and refolding of both the client and the chaperone (Tapley et al, 2010). Another periplasmic chaperone, Spy, finely tunes its affinity for client proteins to enable them to fold while bound to Spy (Stull et al, 2016). This folding buries hydrophobic residues, decreasing client binding and helping favor client release (Koldewey et al, 2016). Here, we show UgpB is a periplasmic chaperone capable of inhibiting bile-mediated protein aggregation and its chaperone activity is tightly regulated by the small molecule G3P.

Our chaperone discovery efforts used a protein folding biosensor-containing *E. coli* strain to find host factors involved in stabilizing destabilized variants of the well-studied model protein Im7. Using this approach, we found that the UgpB serves as a molecular chaperone to prevent generalized bile-induced protein aggregation. UgpB's previously characterized function is that as a periplasmic G3P binding protein (Wuttge et al, 2012). We report here that UgpB has an additional moonlighting activity namely that as a molecular chaperone. Of note, chaperone activity of various bacterial periplasmic substrate-binding proteins, including maltose binding protein (MBP), galactose binding protein (MglB), oligopeptide binding protein (OppA) and dipeptide binding protein (DppA), have previously been observed, implying that at least several

small molecule binding proteins may also play a role in protein folding (Lennon et al, 2015; Richarme & Caldas, 1997). Among these binding proteins, *E. coli* MBP is very commonly fused to recombinant proteins to enhance their solubility and yield (Riggs, 2000). How MBP increases the solubility of the fused protein is still not clear, but one possible explanation is that MBP exerts a cis acting chaperone function when fused to proteins (Fox et al, 2001; Richarme & Caldas, 1997). Interestingly, mutations in the ligand-binding cleft of MBP can dramatically reduce its ability to keep its fusion partner soluble (Fox et al, 2001). Though the chaperone active regions of OppA and DppA have not yet been characterized the co-crystal structure of OppA and DppA with their substrate peptides shows that the peptide is bound in a deep groove in the cleft region (Dunten & Mowbray, 1995; Sleigh et al, 1999).

UgpB appears to have the unusual ability to be able to broadly target bile induced protein aggregation. Though it has been reported that chaperones are induced by bile salts (Bernstein et al, 1999; Cremers et al, 2014; Flahaut et al, 1996; Leverrier et al, 2003; Ruiz et al, 2013), their role in combatting bile induced protein folding had been little studied. We find that none of the well-studied periplasmic chaperones, including SurA, Spy and OsmY, are capable of inhibiting bile salt induced protein aggregation. Several studies highlight the role that bile salts play both in bacterial stress and as environmental cues for signal transduction. One recent study shows that bile salts are involved in virulence gene regulation *Vibrio cholera*. Bile salt mediated denaturation of the transmembrane transcription factor ToxR enhances its ability to interaction with its regulatory protein ToxS triggering activation of virulence gene expression (Midgett et al, 2017). In addition, bile salt-binding to the IpaD needle tip of type III secretion apparatus in *Shigella flexneri* has been shown to induce a conformational change, that results in the recruitment of IpaB which is necessary for the maturation of the complex prior to host cell contact (Dickenson et al, 2011). These are some positive ways that bile salts induce structural changes, but overall bile salts are damaging to proteins, making it not unsurprising that organisms have evolved proteins like UgpB that respond to the threat these potent protein denaturants pose.

Interestingly, it appears that UgpB only functions as a chaperone when it is G3P free. Our structural analysis shows that a deep groove opens up in UgpB when G3P dissociates and consequently, many residues of the core region, including the residues directly associated with G3P interaction, are solvent-exposed. Mutational studies show that UgpB variants of E66A and

R374V, which are defective in G3P binding, function as a constitutively active chaperones. In addition, the two hydrophobic residues, W169 and W172, are involved in G3P binding and likely also in peptide binding (Wuttge et al, 2012) and our results suggest that they are also involved in the chaperone activity of UgpB. Therefore, we propose that G3P and peptides bind to sites on UgpB that at least partially overlap. The overlap of G3P and substrate binding sites could explain why the chaperone activity of UgpB is negatively regulated by G3P binding.

We demonstrate that pH values that mimic those present in the stomach serve to strip off bound G3P, activating UgpB as a chaperone uniquely capable of suppressing bile salt-mediated aggregation of a broad variety of periplasmic proteins. This leads us to speculate that a novel ATP independent cycle exists whereby UgpB uses small molecules present in various intestinal compartments to mediate switching between G3P and chaperone activity in concert with organismal needs. This model is illustrated in figure EV4. Our experiments suggest that stomach acid would likely strip off its bound cofactor, exposing a deep groove on the surface of UpgB. This would likely conveniently activate UgpB as a chaperone apparently just in time for it to respond to the protein aggregation effects of high concentrations of bile that flow into the duodenum, which is the next stop in the journey of an organism through the intestinal tract. These protein denaturation effects of bile however are a temporary issue since as organisms pass into the jejunum, bile salts are diluted out and efficiently absorbed (Heaton, 1969; Weski & Ehrmann, 2012). As this is happening, the degradation of dietary glycerophospholipids acts to raise G3P levels in the intestine (Antonio Blanco, 2017; Ildiko Domonkos, 2015; Wanner, 1996). In the final steps in our proposed model, G3P produced by digestion then binds to UgpB and inactivates its chaperone activity (Figure EV4) and UgpB simultaneously regains its role as a G3P binding protein, allowing G3P to be used as a carbon and phosphate source (Wanner, 1996).

MATERIALS AND METHODS

Bacterial strains, growth conditions, and plasmid constructions

The strains used in this study are listed in Appendix Table S1. All strains used are derivatives of *E. coli* K-12. The strain SQ765 (MG1655 Δ*hsdR*) was used as WT. The Tn5 insertions or deletion alleles from the systematic Keio knockout strain collection were transferred into the MG1655 WT strain by P1 transduction as previously described (Baba et al, 2006; Lennox,

1955). To make multiple gene deletions, the protocol of Baba et al. was followed (Baba et al, 2006). In brief, the single kanamycin insertion mutants were transformed with pCP20, a plasmid encoding a temperature sensitive flippase, which was used to remove the kanamycin resistant cassette from the chromosome, generating a kanamycin sensitive deletion (Baba et al, 2006). Subsequently, additional kanamycin resistant gene insertions were transferred by P1 transduction. NEB10β was used for cloning and maintaining of plasmids. If not otherwise specified, cells were grown at 37°C in Luria Bertani (LB) broth containing appropriate antibiotics, 100 µg/ml ampicillin, 25 µg/ml kanamycin, 34 µg/ml chloramphenicol, and/or 17 µg/ml tetracycline. The *ugpB* gene was cloned into pBAD33 and pTrc99a for use in *in vivo* complementation (Appendix Table S1). For purification purposes, the *ugpB* gene was cloned into pET28a-Sumo and transformed into BL21(DE3). Site-directed mutagenesis was performed as described (QuikChange Site-Directed Mutagenesis Kit - Agilent). Primers and the restriction enzymes used for cloning are described in Appendix Table S2.

Tn-Seq

Transposon mutagenesis was conducted as described by Lai et al. (Lai et al, 2017). In brief, SQ765 pBR322, SQ765 pBR322 *bla*::Im7 L53A I54A, SQ1698 pBR322, and SQ1698 pBR322-*bla*::Im7 L53A I54A were mutagenized with the Ez-Tn5 <Kan-2> transposome (Epicentre). Transposon insertion mutants were isolated by selecting for kanamycin resistance on LB-Kan agar plates at 37°C. Between 7×10^5 and 10^6 colonies were pooled from the LB-Kan plates and suspended in LB broth. Sterilized glycerol was added to the suspension (OD_{600} = ~80) to a final concentration of 16%. The mutant library was stored at −80°C. 140 µl of the mutant library cell stock was inoculated into 50 ml of LB broth and cultured at 37°C with shaking until the OD_{600} = ~1. The library cells were then plated on LB agar with the indicated ampicillin concentrations (as described in the figure legends) and incubated at 37°C for 16 h. The colonies that arose on these LB-ampicillin plates were harvested by scraping and suspended in LB broth.

Tn-seq sequencing libraries were prepared as previously described (Lai et al, 2017). Genomic DNA was extracted from the pooled mutant slurry using the Wizard Genomic DNA Purification Kit (Promega) and fragmented using NEBNext dsDNA Fragmentase (NEB) at 37°C for 25 min. Afterwards, fragmented DNA was purified by using Agencourt AMPure XP beads (Beckman Coulter, Inc.) and eluted into water. Purified fragmented DNA was treated with terminal

deoxynucleotidyl transferase (TdT; Promega) in a reaction with dCTP and ddCTP to add poly-dC at the 3' end of DNA at 37°C for 1 h. TdT was then inactivated at 75°C for 20 min. TdT-treated DNA was purified using a DTR gel filtration cartridge (EdgeBio).

The purified TdT-treated DNA was used as a template for PCR amplification of the transposon junctions by using the Easy-A HiFi Cloning System (Agilent Technologies) and the primers PolyG-1st-1 and Tn5-1st-1 (listed in Appendix Table S2). To amplify the transposon junctions and append the sequencing barcode, a second nested PCR was performed. NEBNext Multiplex Oligos for Illumina (NEB) and Tn5-2nd-1 were used as primers. The final PCR product was electrophoresed on a 2% agarose gel, and fragments ranging from 200-500 bp were cut out and gel purified by using a QIAquick Gel Extraction Kit (Qiagen). The purified libraries were sequenced at the University of Michigan Sequencing Core on a HiSeq 2500 (Illumina) on a single end run.

Sequenced reads were mapped to the *E. coli* MG1655 genome (NCBI NC_000913). The transposon insertion sites were localized and visualized by using the Sanger Artemis Genome Browser and Annotation tool. The fold change enrichment under ampicillin selection conditions relative to LB without ampicillin were calculated as previously described (Lai et al, 2017).

Spot titer assays

Colonies of WT and mutant strains were picked from LB plates containing the appropriate antibiotics, then grown overnight in LB broth also containing appropriate antibiotics with shaking at 37°C. Overnight cultures were diluted 100-fold in LB broth and incubated with shaking at 37°C until the OD_{600} reached 1.0. For *ugpB* complementation from either pBAD30 or pTrc99a vectors (Guzman et al, 1995), 0.2% L-arabinose and 0.2 mM IPTG were added to induce expression of UgpB from pBAD33 and pTrc99A, respectively, when the culture OD_{600} reached 0.3–0.4; incubation continued until the OD_{600} reached 1.0. The cells were diluted 10-fold in the range of 10^{-1} to 10^{-6}, and 3 µl was spotted onto LB plates containing different concentrations of ampicillin. For *ugpB* complementation, 2% L-arabinose or 0.2 mM IPTG supplementation in the LB agar medium was used for the strains containing pBAD33 derivatives and pTrc99a derivatives, respectively. The spotted plates were incubated at 37°C for 12-14 h.

Western blotting

To monitor the levels of β-lactamase and its folding biosensor fusion derivatives, single colonies of strains containing these constructs were grown overnight in LB broth supplemented with the appropriate antibiotics (17 μg/ml tetracycline) at 37°C, diluted 100-fold into LB broth, and incubated to reach OD_{600} 1.0 at 37°C. The harvested cells were resuspended in PBS, disrupted by sonication using Kontes micro ultra sonication cell disruptor on ice, followed by sonication for three cycles of 5 s on ice. The resulting cell lysates were used for Western blotting.

To monitor the levels of the Im7 and Im7 L53A I54A proteins by themselves in the absence of a fusion context, single colonies of strains containing plasmids expressing these strains were inoculated in LB broth with appropriate antibiotics (25 μg/ml kanamycin) and incubated at 37°C overnight. The overnight culture was diluted 100-fold in the LB broth and incubated at 37°C until the cell culture reached an OD_{600} = 0.4. Im7 expression was then induced by 5 mM IPTG for 1 h, and a periplasmic extract was performed as previously described (Quan et al, 2013; Quan et al, 2011). These cell extracts were subjected to SDS-PAGE (Nu-PAGE, Invitrogen) and subsequently blotted onto a polyvinylidene difluoride membrane (Trans-blot Turbo, Biorad). Transferred membranes were incubated in blocking solution (1 × Tris-buffered saline (TBS) pH 7.4, 0.01% Tween 20, 5% bovine serum albumin) for 1 h at room temperature, then incubated with antibodies at 4°C overnight. Anti-β-lactamase antibody (Millipore, AB-3738) and anti-Im7 (lab collection, Pacific Immunology, Appendix Figure S14) were used, with anti-maltose binding protein (MBP) (New England Biolabs, E8032S) serving as a loading control. After washing with 1 × Tris-buffered saline (TBS) pH 7.4, 0.01% Tween 20 (washing buffer), secondary antibodies (IRDye 680LT goat anti-rabbit/ 800CW goat anti-mouse, LI-COR) were added and allowed to bind for 2 h at room temperature. The membranes were then washed with washing buffer and visualized by using the LI-COR imaging system.

Periplasmic extraction

Periplasmic extracts were performed using the polymyxin B method as described previously (Quan et al, 2013). Briefly, 4 OD_{600} units of cells were harvested and resuspended in 100 μl of polymyxin buffer (50 mM Tris HCl, pH 7.5, 5 mM EDTA, 150 mM NaCl, 1 mg/ml polymyxin B sulfate). The cell resuspensions were incubated on ice for 1 h and centrifuged at 16,000 *g* for 30 min at 4°C. The supernatant served as the periplasmic fraction.

β-lactamase assay

To monitor β-lactamase activity *in vitro*, the strains harboring expression vectors encoding Im7 L53A I54A fused β-lactamase constructs (CL198, CL248, CL249, and CL250) were streaked on LB agar plates containing 17 μg/ml tetracycline. Single colonies of these strains were used to innoculate 5 ml 37°C overnight cultures in LB broth containing 17 μg/ml tetracycline, diluted 100-fold in LB broth, and incubated at 37°C until the OD_{600} reached 1.0. Harvested cells were either resuspended in 50 mM sodium phosphate buffer pH 6.0 and disrupted by sonication on ice or fractionated to obtain periplasmic fractions.

For the activity assays, 4 μg of the periplasmic extracts were diluted into 90 μl of 50 mM sodium phosphate buffer pH 6.0, and 5 μl of a 0.5 mM nitrocefin stock solution (Millipore) was added. Hydrolysis of the β-lactamase substrate nitrocefin was detected by the increase in absorbance at 486 nm over time using a 96-well plate reader at 37ºC. β-lactamase activity was normalized to the activity of β-lactamase present in the parental CL198 strain.

Proteome analysis

CL198, CL248, and CL249 strains were streaked on LB agar plates containing tetracycline. Single colonies of these strains were grown overnight in LB broth with tetracycline at 37°C, then diluted 100-fold into LB broth and incubated at 37°C until the OD_{600} reached 1.0. 40 ml of these late log phase cells were then harvested by centrifugation at 3,000 *g* for 10 min. The cell pellets were washed twice in 40 ml of phosphate buffered saline (137 mM NaCl, 2.7 mM KCl, 10 mM Na_2HPO_4, 1.8 mM KH_2PO_4, pH 7.4). The cell pellets were frozen in liquid nitrogen and then stored at −80°C. The cell pellets were provided to MS Bioworks (Ann Arbor), who performed mass spectroscopy analysis as described (Yan et al, 2019).

Protein purification

UgpB was purified as described previously (Quan et al, 2011).

Protein denaturation and renaturation

To remove tightly bound cofactors, purified UgpB was subjected to a denaturation/renaturation procedure (Wuttge et al, 2012). UgpB was dialyzed against 1 l of denaturing buffer (50 mM Tris HCl pH 7.5, 10 mM DTT, 6 M guanidine hydrochloride) overnight at 4°C. UgpB was then renatured by dialysis against 1 l of renaturing buffer (50 mM Tris HCl, pH 7.5) over 4 days, with

two buffer changes per day. The renatured proteins were exchanged into 40 mM HEPES pH 7.5 by five cycles of concentration and dilution with 10 kDa cut-off Amicon centrifugal filter columns.

Isothermal titration calorimetry (ITC)

All protein samples were dialyzed against a common solution of 40 mM HEPES KOH, pH 7.5. ITC was performed with a MicroCal iTC200 using the same buffer at 10°C. 40 μM of $UgpB_{G3P}$/apo UgpB were titrated with 400 μM G3P. 1.0 μl injections were used for the titrations. ITC thermograms were fitted to a one-site model with the Origin software that is provided with the instrument.

Circular dichroism (CD)

Far-UV CD spectra were recorded from 200–250 nm at 25°C in a Jasco J-1500 spectropolarimeter. To monitor conformational changes due to G3P binding, the CD spectra of 10 μM UgpB and $UgpB_{G3P}$ in 50 mM sodium phosphate buffer at pH 6.0 were compared. The spectra of 2 μM UgpB incubated in 10 mM sodium phosphate buffer at pH 2.0 or 7.0 were compared to monitor acid-dependent denaturation.

Fluorescence emission spectra of tryptophan

UgpB has eight tryptophan residues. 2 μM of UgpB was used to monitor the fluorescence emission spectra of tryptophan. 40 mM HEPES pH 7.5 buffer was used to monitor G3P binding after renaturation. 40 mM KH_2PO_4 KOH pH 7.5 buffer was used to monitor G3P binding in the presence of bile salts and during the pH transition simulation. Tryptophan fluorescence was excited at 295 nm, and emission spectra were recorded from 300–400 nm at 25°C using a Cary Eclipse fluorescence spectrophotometer.

Aggregation assays

CHO-induced aggregation was monitored by light scattering at 25°C. 12 μM MDH (Roche) was used in 40 mM KH_2PO_4 KOH pH 7.5 buffer containing 15 mM CHO. Light scattering was monitored at 360 nm using a Cary Eclipse fluorimeter in the absence or presence of increasing concentrations of UgpB.

Protein supernatant/pellet assay for bile-induced protein aggregation

Bile salt-induced protein aggregation was monitored by a supernatant/pellet assay. 12 μM MDH (Roche), 12 μM CS (Sigma), 12 μM LDH (Roche), or 800 μg soluble total lysate from the SQ765 strain were used. 15 mM CHO (Sigma) was used for MDH and CS, and 50 mM CHO was used for LDH and total lysate. 40 mM KH_2PO_4 KOH pH 7.5 were used for the CHO aggregation assay. Different ratios of UgpB or MBP proteins were added as described. To determine the effect of G3P binding to UgpB, 120 μM of G3P was added to the reaction buffers of MDH and LDH, and 60 and 600 μM of G3P was added to the reaction buffers of CS and total lysate, respectively. G3P was added before adding either UgpB or MBP into the buffer. Aggregation reactions were performed at 37°C for the described time. After incubation, the samples were centrifuged at 16,000 *g* for 20 min at 4°C to separate supernatant and pellet fractions. The pellet was washed with ice cold distilled water and centrifuged again at 16,000 *g* for 20 min at 4°C. The pellet was resuspended in SDS-PAGE protein sample buffer, which is 5-fold concentrated for MDH and CS and 10-fold concentrated for LDH and total lysate. Both supernatant and pellet fractions were analyzed by SDS-PAGE and visualized by Coomassie staining.

pH transition experiment

3 mM of $UgpB_{G3P}$ was incubated with 3 mM G3P for 5 min at room temperature to allow for complete ligand binding. The incubated $UgpB_{G3P}$ was added to 10 ml of either 10 mM NaH_2PO_4 HCl pH 2.0 or 10 mM NaH_2PO_4 NaOH pH 7.0 to attain a final protein concentration of 5 μM and then kept at room temperature for 20 min. To flush the released G3P, buffer was exchanged four times by centrifuging at 3,500 rpm at room temperature using Amicon 3 kDa cut-off centrifugal tubes. 100X stock (1M NaH_2PO_4 NaOH pH 7.0) was added to neutralize pH 2.0 to pH 7.0. Buffer was exchanged with 10 mM NaH_2PO_4 NaOH pH7 by centrifuging at 3,500 rpm at room temperature using Amicon 30 kDa cut-off centrifugal tubes. The proteins were centrifuged at 16,000 *g* for 20 min at 4°C, and the soluble supernatant fraction was used to monitor G3P binding by observing tryptophan fluorescence upon addition of G3P.

Crystallization and structure determination

The microcrystals were initially obtained at 20°C by sitting-drop vapor diffusion with 1 μl of 90 mg ml^{-1} UgpB (W169S/W172S) mixed with an equal volume of reservoir solution containing

100mM CHES (pH 7.5) and 30% PEG400. A 2-µl drop containing microcrystals of UgpB was diluted into a 50-µl mother reservoir solution, vortexed with the stainless steel beads (Hampton), then 1000-fold diluted to the mother reservoir solution to obtain the seed stock. Well-diffracting crystals were grown at 20°C by hanging-drop vapor diffusion with 1.5 µl of 90 mg ml^{-1} UgpB (W169S/W172S), 2 µl of the reservoir solution mentioned above and 0.5 µl of seed stock. Crystals were cryoprotected in the crystallization condition supplemented with 25% glycerol and then flash-cooled in liquid nitrogen.

The diffraction data were collected at beamline X06DA-PXIII at the Swiss Light Source (SLS) and were processed using XDS. The structure was solved by molecular replacement using PHENIX MR with individual domains (N-terminal domain including residues 1-122 and 282-359, and C-terminal domain including residues 123-281 and 360-415) of the G3P-bound structure (pdb: 4aq4) as searching models. Multiple rounds of manual model rebuilding and refinement of the structure were carried out in Coot and PHENIX Refine program. Statistics of X-ray structure determination are listed in Appendix Table S3.

Protein-peptide docking

The docking experiments were performed with UgpB and 24 MDH peptides using MDOCKPEP server (http://zougrouptoolkit.missouri.edu/mdockpep/) (Xu et al, 2018). Sequence of MDH peptides used in this work can be found in Dataset EV2. The default values of parameters were used in the docking simulation.

DATA AVAILABILITY

The coordinates and structure factors for the UgpB structure have been deposited in the Protein Data Bank (http://www.pdb.org) under accession number 6X84.

ACKNOWLEDGMENTS

We thank Thao Truong and Thomas Bernhardt from Harvard Medical School for offering a protocol for Tn-Seq and for providing much helpful experimental advice and comments on the manuscript. We also thank Frederick Stull for helpful discussion and comments on the manuscript. We thank Risav Mitra for advice on peptide docking, Dr. Vincent Olieric for the

help with the session setup at the Swiss Light Source and all members of the Bardwell and Jakob labs for useful discussions. The Howard Hughes Medical Institute funded this work. Support of this work by the Swiss National Science Foundation (grants 310030B_176403/1 and 31003A_156304 to R.G.) is also gratefully acknowledged.

AUTHOR CONTRIBUTIONS

C.L. and J.C.A.B. conceived this study, designed the research, interpreted the data, and wrote and edited the manuscript. C.L., P.B. and K.W. performed the experiments and data analysis. D.Z. helped in the collection and analysis of X-ray diffraction data and R.G. supervised D.Z. and provided access to the Swiss Light Source at the Paul Scherrer Institute.

CONFLICT OF INTERESTS

The authors declare no competing interests.

REFERENCES

Antonio Blanco GB (2017) *Chapter 5. Lipids*: Elsevier.

Baba T, Ara T, Hasegawa M, Takai Y, Okumura Y, Baba M, Datsenko KA, Tomita M, Wanner BL, Mori H (2006) Construction of Escherichia coli K-12 in-frame, single-gene knockout mutants: the Keio collection. *Molecular systems biology* **2:** 2006 0008

Balch WE, Morimoto RI, Dillin A, Kelly JW (2008) Adapting proteostasis for disease intervention. *Science* **319:** 916-919

Bernstein C, Bernstein H, Payne CM, Beard SE, Schneider J (1999) Bile salt activation of stress response promoters in Escherichia coli. *Curr Microbiol* **39:** 68-72

Burby PE, Nye TM, Schroeder JW, Simmons LA (2017) Implementation and Data Analysis of Tn-seq, Whole-Genome Resequencing, and Single-Molecule Real-Time Sequencing for Bacterial Genetics. *Journal of bacteriology* **199**

Cabral DJ, Small DM, Lilly HS, Hamilton JA (1987) Transbilayer movement of bile acids in model membranes. *Biochemistry* **26:** 1801-1804

Cremers CM, Knoefler D, Vitvitsky V, Banerjee R, Jakob U (2014) Bile salts act as effective protein-unfolding agents and instigators of disulfide stress in vivo. *Proceedings of the National Academy of Sciences of the United States of America* **111:** E1610-1619

Crepin S, Lamarche MG, Garneau P, Seguin J, Proulx J, Dozois CM, Harel J (2008) Genome-wide transcriptional response of an avian pathogenic Escherichia coli (APEC) pst mutant. *BMC genomics* **9:** 568

Dahl JU, Koldewey P, Salmon L, Horowitz S, Bardwell JC, Jakob U (2015) HdeB functions as an acid-protective chaperone in bacteria. *The Journal of biological chemistry* **290:** 9950

Dickenson NE, Zhang L, Epler CR, Adam PR, Picking WL, Picking WD (2011) Conformational changes in IpaD from Shigella flexneri upon binding bile salts provide insight into the second step of type III secretion. *Biochemistry* **50:** 172-180

Dunten P, Mowbray SL (1995) Crystal structure of the dipeptide binding protein from Escherichia coli involved in active transport and chemotaxis. *Protein science : a publication of the Protein Society* **4:** 2327-2334

Fenn JS, Nepravishta R, Guy CS, Harrison J, Angulo J, Cameron AD, Fullam E (2019) Structural Basis of Glycerophosphodiester Recognition by the Mycobacterium tuberculosis Substrate-Binding Protein UgpB. *ACS chemical biology* **14:** 1879-1887

Flahaut S, Frere J, Boutibonnes P, Auffray Y (1996) Comparison of the bile salts and sodium dodecyl sulfate stress responses in Enterococcus faecalis. *Applied and environmental microbiology* **62:** 2416-2420

Foit L, Morgan GJ, Kern MJ, Steimer LR, von Hacht AA, Titchmarsh J, Warriner SL, Radford SE, Bardwell JC (2009) Optimizing protein stability in vivo. *Molecular cell* **36:** 861-871

Fox JD, Kapust RB, Waugh DS (2001) Single amino acid substitutions on the surface of Escherichia coli maltose-binding protein can have a profound impact on the solubility of fusion proteins. *Protein science : a publication of the Protein Society* **10:** 622-630

Gardner SG, Miller JB, Dean T, Robinson T, Erickson M, Ridge PG, McCleary WR (2015) Genetic analysis, structural modeling, and direct coupling analysis suggest a mechanism for phosphate signaling in Escherichia coli. *BMC genetics* **16 Suppl 2:** S2

Goto Y, Calciano LJ, Fink AL (1990) Acid-induced folding of proteins. *Proceedings of the National Academy of Sciences of the United States of America* **87:** 573-577

Gunn JS (2000) Mechanisms of bacterial resistance and response to bile. *Microbes and infection* **2:** 907-913

Guzman LM, Belin D, Carson MJ, Beckwith J (1995) Tight regulation, modulation, and high-level expression by vectors containing the arabinose PBAD promoter. *Journal of bacteriology* **177:** 4121-4130

Hartl FU, Bracher A, Hayer-Hartl M (2011) Molecular chaperones in protein folding and proteostasis. *Nature* **475:** 324-332

Heaton KW (1969) The importance of keeping bile salts in their place. *Gut* **10:** 857-863

Hernandez SB, Cota I, Ducret A, Aussel L, Casadesus J (2012) Adaptation and preadaptation of Salmonella enterica to Bile. *PLoS genetics* **8:** e1002459

Ildiko Domonkos MK, Zoltan Gombos (2015) Versatile roles of lipids and carotenoids in membranes. *Acta Biologica Szegediensis* **59:** 22

Koldewey P, Stull F, Horowitz S, Martin R, Bardwell JCA (2016) Forces Driving Chaperone Action. *Cell* **166:** 369-379

Lai GC, Cho H, Bernhardt TG (2017) The mecillinam resistome reveals a role for peptidoglycan endopeptidases in stimulating cell wall synthesis in Escherichia coli. *PLoS Genet* **13:** e1006934

Lemieux MJ, Huang Y, Wang DN (2004) Glycerol-3-phosphate transporter of Escherichia coli: structure, function and regulation. *Research in microbiology* **155:** 623-629

Lennon CW, Thamsen M, Friman ET, Cacciaglia A, Sachsenhauser V, Sorgenfrei FA, Wasik MA, Bardwell JC (2015) Folding Optimization In Vivo Uncovers New Chaperones. *Journal of molecular biology* **427:** 2983-2994

Lennox ES (1955) Transduction of linked genetic characters of the host by bacteriophage P1. *Virology* **1:** 190-206

Leverrier P, Dimova D, Pichereau V, Auffray Y, Boyaval P, Jan G (2003) Susceptibility and adaptive response to bile salts in Propionibacterium freudenreichii: physiological and proteomic analysis. *Applied and environmental microbiology* **69:** 3809-3818

Merritt ME, Donaldson JR (2009) Effect of bile salts on the DNA and membrane integrity of enteric bacteria. *Journal of medical microbiology* **58:** 1533-1541

Midgett CR, Almagro-Moreno S, Pellegrini M, Taylor RK, Skorupski K, Kull FJ (2017) Bile salts and alkaline pH reciprocally modulate the interaction between the periplasmic domains of Vibrio cholerae ToxR and ToxS. *Molecular microbiology* **105:** 258-272

Nichols RJ, Sen S, Choo YJ, Beltrao P, Zietek M, Chaba R, Lee S, Kazmierczak KM, Lee KJ, Wong A, Shales M, Lovett S, Winkler ME, Krogan NJ, Typas A, Gross CA (2011) Phenotypic landscape of a bacterial cell. *Cell* **144:** 143-156

Olive AJ, Kenjale R, Espina M, Moore DS, Picking WL, Picking WD (2007) Bile salts stimulate recruitment of IpaB to the Shigella flexneri surface, where it colocalizes with IpaD at the tip of the type III secretion needle. *Infect Immun* **75:** 2626-2629

Prieto AI, Ramos-Morales F, Casadesus J (2004) Bile-induced DNA damage in Salmonella enterica. *Genetics* **168:** 1787-1794

Quan S, Hiniker A, Collet JF, Bardwell JC (2013) Isolation of bacteria envelope proteins. *Methods Mol Biol* **966:** 359-366

Quan S, Koldewey P, Tapley T, Kirsch N, Ruane KM, Pfizenmaier J, Shi R, Hofmann S, Foit L, Ren G, Jakob U, Xu Z, Cygler M, Bardwell JC (2011) Genetic selection designed to stabilize proteins uncovers a chaperone called Spy. *Nature structural & molecular biology* **18:** 262-269

Richarme G, Caldas TD (1997) Chaperone properties of the bacterial periplasmic substrate-binding proteins. *The Journal of biological chemistry* **272:** 15607-15612

Riggs P (2000) Expression and purification of recombinant proteins by fusion to maltose-binding protein. *Molecular biotechnology* **15:** 51-63

Ruiz L, Margolles A, Sanchez B (2013) Bile resistance mechanisms in Lactobacillus and Bifidobacterium. *Front Microbiol* **4:** 396

Sleigh SH, Seavers PR, Wilkinson AJ, Ladbury JE, Tame JR (1999) Crystallographic and calorimetric analysis of peptide binding to OppA protein. *Journal of molecular biology* **291:** 393-415

Stull F, Betton JM, Bardwell JCA (2018) Periplasmic Chaperones and Prolyl Isomerases. *EcoSal Plus* **8**

Stull F, Koldewey P, Humes JR, Radford SE, Bardwell JCA (2016) Substrate protein folds while it is bound to the ATP-independent chaperone Spy. *Nature structural & molecular biology* **23:** 53-58

Tapley TL, Franzmann TM, Chakraborty S, Jakob U, Bardwell JC (2010) Protein refolding by pH-triggered chaperone binding and release. *Proceedings of the National Academy of Sciences of the United States of America* **107:** 1071-1076

Urdaneta V, Casadesus J (2017) Interactions between Bacteria and Bile Salts in the Gastrointestinal and Hepatobiliary Tracts. *Frontiers in medicine* **4:** 163

van Opijnen T, Bodi KL, Camilli A (2009) Tn-seq: high-throughput parallel sequencing for fitness and genetic interaction studies in microorganisms. *Nature methods* **6:** 767-772

Wanner BL (1996) *Phosphorus assimilation and control of the phosphate regulon. In Escherichia coli and Salmonella*, Washington, DC.: American Society for Microbiology.

Weski J, Ehrmann M (2012) Genetic analysis of 15 protein folding factors and proteases of the Escherichia coli cell envelope. *Journal of bacteriology* **194:** 3225-3233

Wuttge S, Bommer M, Jager F, Martins BM, Jacob S, Licht A, Scheffel F, Dobbek H, Schneider E (2012) Determinants of substrate specificity and biochemical properties of the sn-glycerol-3-phosphate ATP binding cassette transporter (UgpB-AEC2) of Escherichia coli. *Molecular microbiology* **86:** 908-920

Xu X, Yan C, Zou X (2018) MDockPeP: An ab-initio protein-peptide docking server. *Journal of computational chemistry* **39:** 2409-2413

Yan Z, Hussain S, Wang X, Bernstein HD, Bardwell JCA (2019) Chaperone OsmY facilitates the biogenesis of a major family of autotransporters. *Molecular microbiology*

FIGURE LEGENDS

Figure 1. Genetic Screening Using Tn-Seq and a Protein Folding Sensor

(A) As a protein folding sensor, we constructed a tripartite fusion protein in which the test protein (shown in blue) is inserted between the N-terminal portion of the selectable marker, β-lactamase (shown in pink), and the C-terminal portion of β-lactamase (shown in peach). Instability of the test protein leads to either degradation or aggregation, resulting in lower ampicillin resistance (Amp^S) of strains containing this biosensor compared to those in which the test protein is stable. If a host factor or chaperone such as Spy stabilizes the test protein, higher levels of ampicillin resistance (Amp^R) will be exhibited. First, we generated a transposon (Tn) library in strains containing either a protein folding sensor or a β-lactamase glycine-serine linker construct (see Methods for details). Secondly, ampicillin resistance selections were performed, and colonies resistant to various levels of ampicillin were pooled and subjected to deep sequencing. This enabled the genomic mapping of the position and frequency of transposon insertion sites. Genes showing an altered transposon insertion frequency in the presence of a protein folding sensor were selected as candidates for host factors that affect the stability of that protein folding sensor. See also Appendix Figure S1A.

(B) When transposon insertion libraries subjected to ampicillin resistance selection, a substantial increase in transposon insertion frequency in the *pstSCA* genes was observed in strains containing the protein folding sensor (pBR322 *bla*::Im7 L53A I54A) relative to a strain containing just pBR322. Transposon insertion frequency increased 21-, 24-, and 8-fold in the

pstS, *pstA*, and *pstC* genes, respectively, compared to the insertion frequency found with no ampicillin selection.

Figure 2. Deletion Mutants in the *pstSCA* Genes Act to Stabilize the β-lactamase-Im7 L53A I54A Folding Biosensor and the Im7 L53A I54A Protein Itself *In Vivo*

(A) To verify that disruption of the *pst* genes is sufficient to increase ampicillin resistance of strains containing the pBR322 *bla*::Im7 L53A I54A folding biosensor and to test which of the genes in the *pst* operon are sufficient for this effect, pBR322 and pBR322 *bla*::Im7 L53A I54A were transformed into strains containing in-frame deletion mutants of each of the *pst* genes (*pstS*, *pstC*, and *pstA*, respectively). The deletion mutants of each of these *pst* genes showed higher ampicillin resistance than did the WT strain MG1655 in the presence of pBR322 *bla*::Im7 L53A I54A, but did not shower higher ampicillin resistance in the presence of pBR322. See also Appendix Figure S2A.

(B) Levels of β-lactamase (Bla) and β-lactamase-Im7 L53A I54A were detected by Western blotting using a polyclonal antibody recognizing β-lactamase in the WT strain MG1655 and in isogenic strains containing insertions in the *pstSCA* genes (CL248 (*pstS*::Tn5), CL249 (*pstC*::Tn5), CL250 (*pstA*::Tn5)). Maltose binding protein (MBP) was used as a control.

(C) β-lactamase enzymatic activities present in periplasmic extracts of the Im7 folding biosensor were monitored in *pst* WT and *pst*SCA mutant strains using a spectrophotometric assay. Data are represented as mean ± SEM from three technical replicates (unpaired t-test,** $P<0.01$, *** $P<0.001$ comparison to MG1655; ns, not significant).

(D) To test if levels of the Im7 L53A I54A protein itself, in the absence of the fusion, were also higher in the *pstA* mutant, expression of the Im7 L53A I54A protein from the IPTG-inducible plasmid pCDFTrc was induced using IPTG concentrations ranging from 0–5 mM. Periplasmic fractions were isolated and examined by SDS-PAGE and subsequent Coomassie staining to determine overall protein expression patterns. Im7 L53A I54A levels were determined by Western blotting using an antibody for Im7. MBP was used as a loading control. Im7 L53A I54A was increased in the *pstA* strain relative to the WT control strain. Coomassie staining revealed that a number of periplasmic proteins, including UgpB, were also induced in the *pstA* strain.

Data information: These experiments were repeated twice with similar results and one representative is shown.

Figure 3. UgpB Confers High Ampicillin Resistance to Strains Containing the Destabilized Protein Im7 L53A I54A

(A) MG1655 WT, single mutants of *pstA* and *ugpB*, and a double mutant of *pstA ugpB* were transformed with pBR322 and various pBR322-based folding biosensor constructs. The transformants were examined by a spot titer assay on LB agar plates containing various ampicillin concentrations. Strains containing pBR322 *bla*::Im7 L53A I54A gain considerable ampicillin resistance in the presence of a *pstA* mutation (compare uppermost left and right panels). This resistance is completely lost upon transducing in a *ugpB* mutation (compare next panels down), showing that *ugpB* is responsible for the resistance gained by the *pstA* mutation.
(B) Ampicillin sensitivity conferred by a *ugpB* deletion mutant (CL543) is complemented by UgpB expression from the arabinose inducible expression vector pBAD33 *ugpB* (pCL1).
(C) UgpB expression is sufficient to lead to higher levels of Im7 L53A I54A protein. Im7 L53A I54A and UgpB were expressed in a *ugpB* mutant strain (CL543) from pCDFTrc and pTrc99a vectors, respectively, both of which have an IPTG-inducible promoter. Periplasmic fractions were isolated and examined by Western blotting. "-" indicates strains containing empty vector and "+" indicates strains containing a recombinant plasmid encoding either Im7 L53A I54A or UgpB. MBP was used as a loading control. Data information: These experiments were repeated twice with similar results and one representative is shown.

Figure 4. UgpB Prevents Bile-Induced Protein Aggregation

(A) UgpB overexpression confers bile salt resistance, and a *ugpB* deletion mutant is slightly CHO sensitive.
(B) CHO-induced MDH protein aggregation analyzed by monitoring light scattering.
(C) CHO-induced MDH protein aggregation analyzed by a solubility assay using centrifugation (cfg) at 16,000 *g* for 20 min. The supernatant (Sup) represents the soluble fraction and the pellet the insoluble fraction; 12 μM MDH was used as a model aggregation-prone substrate (see Methods). Addition of increasing quantities of UgpB increasingly solubilizes MDH. The molar

ratios of MDH:UgpB that were used (left to right) are as follows: 1:0, 1:0.1, 1:0.2, 1:0.5, and 1:1. 5-fold more of the pellet fraction was loaded relative to the supernatant fraction.
(D) The supernatant/pellet assay was performed using a 1:1 MDH:chaperone ratio for Spy, SurA, and OsmY. The pellet fraction was concentrated 5-fold.
(E) 12 μM of MDH alone and a 1:1 ratio of either MDH:UgpB or MDH:MBP were incubated at 37°C for 60 min in the presence of CHO and then fractionated via centrifugation for use in a solubility assay as described above (C) . The pellet fraction was concentrated 5-fold. In some samples (+G3P), 120 μM of G3P was added prior to the addition of any other protein. Addition of G3P inactivates UgpB's ability to inhibit protein aggregation.
(F) 800 μg of *E. coli* total lysate and 60 μM of UgpB/MBP were used for the supernatant/pellet assay. 600 μM of G3P was added before adding proteins. The pellet fraction was concentrated 10-fold. As before, addition of UgpB inhibited aggregation, but only in the absence of G3P.
(G) The anti-aggregation activity of tryptophan single mutant (W169S) and double mutant (W169S/W172S) was examined by CHO-induced MDH aggregation assay. Light scattering values were monitored.
(H) Solubility of MDH is also monitored by supernatant/pellet assay. Tryptophan mutants exhibit constitutively active chaperone function independent of the presence of G3P. The pellet fraction was concentrated 5-fold. 12 μM of MDH and 1:1 ratio of MDH:UgpB proteins and 120 μM of G3P were used.
(I) The anti-aggregation activity of the UgpB variants (E66A and R374V) was examined by CHO-induced MDH aggregation assay. CHO-induced MDH protein aggregation analyzed by monitoring light scattering.
(J) Solubility of MDH is also monitored by supernatant/pellet assay. 12 μM of MDH alone and a 1:1 ratio of MDH:UgpB proteins, 120 μM of G3P were used.
15 mM CHO were used for all the aggregation and supernatant/pellet assays.
Data information: These experiments were repeated at least twice with similar results and one representative is shown.

Figure 5. Structural analysis of G3P-regulated conformational change

(A) Stereoview of a superposition the structure of apo form of UgpB (blue) and the G3P-bound form of UgpB (orange; pdb: 4aq4) is shown. The apo form of UgpB was modeled by SWISS-MODEL program using the 1.25 Å crystal structure of the non G3P binding W169S, W172S variant of UgpB as a template. The C-terminal domains (residues 123-281 and 360-415) of apo UgpB and G3P-bound UgpB were superimposed to illustrate the G3P-induced repositioning of a domain relative to the other.

(B) Apo form exists in a closed conformation and the G3P-binding site is buried in between the two domains (right). G3P-bound form adopts an open conformation and exposes a cleft in the domain interface (left). The surface of UgpB are colored cyan and a continuous groove that buried in closed form but exposed in the open conformation are highlighted according to the characteristics of residues (green, hydrophobic residues; orange, polar residues; blue, positive-charged residues; red, negative charged residues). The enlargement shows the position of residues E66, W169, W172 and R374.

Figure 6. pH Transition Can Activate UgpB's Chaperone Activity

(A) Acid denatures UgpB. The secondary structure of 2 μM UgpB was monitored by circular dichroism (CD) spectroscopy in 10 mM sodium phosphate buffer at pH 2 and pH 7.

(B) G3P binds to acid-stripped UgpB as observed by monitoring the tryptophan fluorescence spectrum, either at pH7 or after transition from pH 2 to 7 (see Methods). Transitions from pH 2 to 7 in the presence of G3P are accompanied by a blue shift, indicating G3P binding.

(C) The anti-aggregation activity of UgpB is monitored by CHO-induced MDH aggregation assay. Light scattering values were monitored. The anti-aggregation activity of UgpB is activated after transition from pH 2 to 7 and the addition of G3P (120 μM) can again inactivate its chaperone activity.

(D) Addition of G3P to UgpB inhibits its anti-aggregation chaperone activity. 12 μM of MDH and a 1:1 ratio of UgpB:MDH were used in a CHO-induced aggregation assay. At 30 min, the indicated concentrations of G3P were added to solutions containing MDH, and MDH aggregation was monitored by light scattering. Note that G3P binding to UgpB still occurs in the presence of 15 mM CHO as monitored by tryptophan fluorescence (inset and Appendix Figure S9).

Data information: These experiments were repeated twice with similar results and one representative is shown.

EXPANDED VIEW FIGURE LEGENDS

Figure EV1. Rediscovery of the chaperone Spy by using Tn-Seq

(A) Transposon insertions resistant to 1.5 mg/ml of ampicillin were selected in both the WT strain MG1655 and its isogenic *baeS*-R426S derivative; both strains harbored the plasmid pBR322. Both of these strains were significantly ampicillin sensitive at this ampicillin concentration, showing about one log of killing (see Appendix Figure S1). An overall decrease in the number of transposon insertions in the WT strain MG1655 in the presence of ampicillin was observed, likely reflecting the ~1 log killing induced by the antibiotic, but there is no substantial decrease in insertions the *spy* and *baeSR* genes relative to adjacent genes.

(B) Transposon insertion libraries selected on 0.7 and 1.2 mg/ml of ampicillin, respectively, were made in the MG1655 WT and *baeS*-R426S strains harboring a protein folding sensor pBR322 *bla*::Im7 L53A I54A. A dramatic decrease in transposon insertions in the *spy* and *baeSR* genes was observed in the *baeS*-R426S mutant strain relative to the insertion frequency found in WT strains, consistent with the known role of Spy, which is overproduced in the *baeS*-R426S strain, in stabilizing the Im7 portion of the folding biosensor.

Figure EV2. UgpB inhibits CHO-induced protein aggregation more effectively when in the G3P-free form.

(A-C) (A) $UgpB_{G3P}$, which has ~90% G3P binding occupancy, was mixed with MDH incubated in 40 mM KH_2PO_4 KOH pH 7.5 buffer in the presence of 15 mM CHO at 37°C for 60 min and then centrifuged at 16,000 *g* for 20 min at 4°C to separate soluble and insoluble fractions (see Methods). Similar experiments were performed with G3P-free UgpB (B) and MBP (C). 12 μM

MDH was used and 1:1, 1:2, 1:4, 1:5, and 1:10 molar ratios of MDH:$UgpB_{G3P}$/UgpB/MBP were used.

(D) A similar experiment was performed using 800 μg of *E. coli* total lysate; 60 μM of $UgpB_{G3P}$ /UgpB were used for the supernatant/pellet assay.

(E) 12 μM of MDH and a 1:1 ratio of UgpB:MDH were used for the CHO-induced aggregation assay. 15 mM CHO were used and the mixtures were incubated at 37°C. At 30 min, the 120 μM, 1.2 mM and 2.4 mM of G3P were added to the solutions containing the described proteins. After further 30 min incubation, soluble and insoluble fractions were separated (see Methods). Overall, experiment setting is same as figure 6D. The solubility of MDH or UgpB itself is not affected by the addition of G3P. The addition of G3P into MDH and UgpB mixture leads the aggregation of MDH, suggesting G3P compete with MDH. Of note, UgpB is also aggregated to some extent. This result may suggest that UgpB is vulnerable to CHO exposure during the dissociation step.

Data information: These experiments were repeated twice with similar results and one representative is shown.

Figure EV3. Docking results for 24 different MDH peptides binding to UgpB.

The best docked models with the lowest energy score for each peptide-docking complex with (A) apo UgpB and (B) holo UgpB are shown. Peptide sequence information and energy score is described in Dataset EV2.

Figure EV4. Speculative Model of UgpB in the Digestive Tract

Enteric bacteria encounter host defense systems including gastric acid in the stomach and bile salts in the duodenum. Periplasmic UgpB unfolds in response to low pH present in the stomach, releasing any bound G3P. This activates UgpB as a molecular chaperone, allowing it to protect periplasmic proteins from the bile-induced aggregation in the duodenum. Upon transition into the jejunum and ileum, the bile concentration declines (Heaton, 1969; Weski & Ehrmann, 2012), and digestion of food substances increases G3P levels. These increasing G3P levels inactivate UgpB as a molecular chaperone and it transitions into its role as a periplasmic G3P-binding protein, which helps to transport G3P into the cytosol.

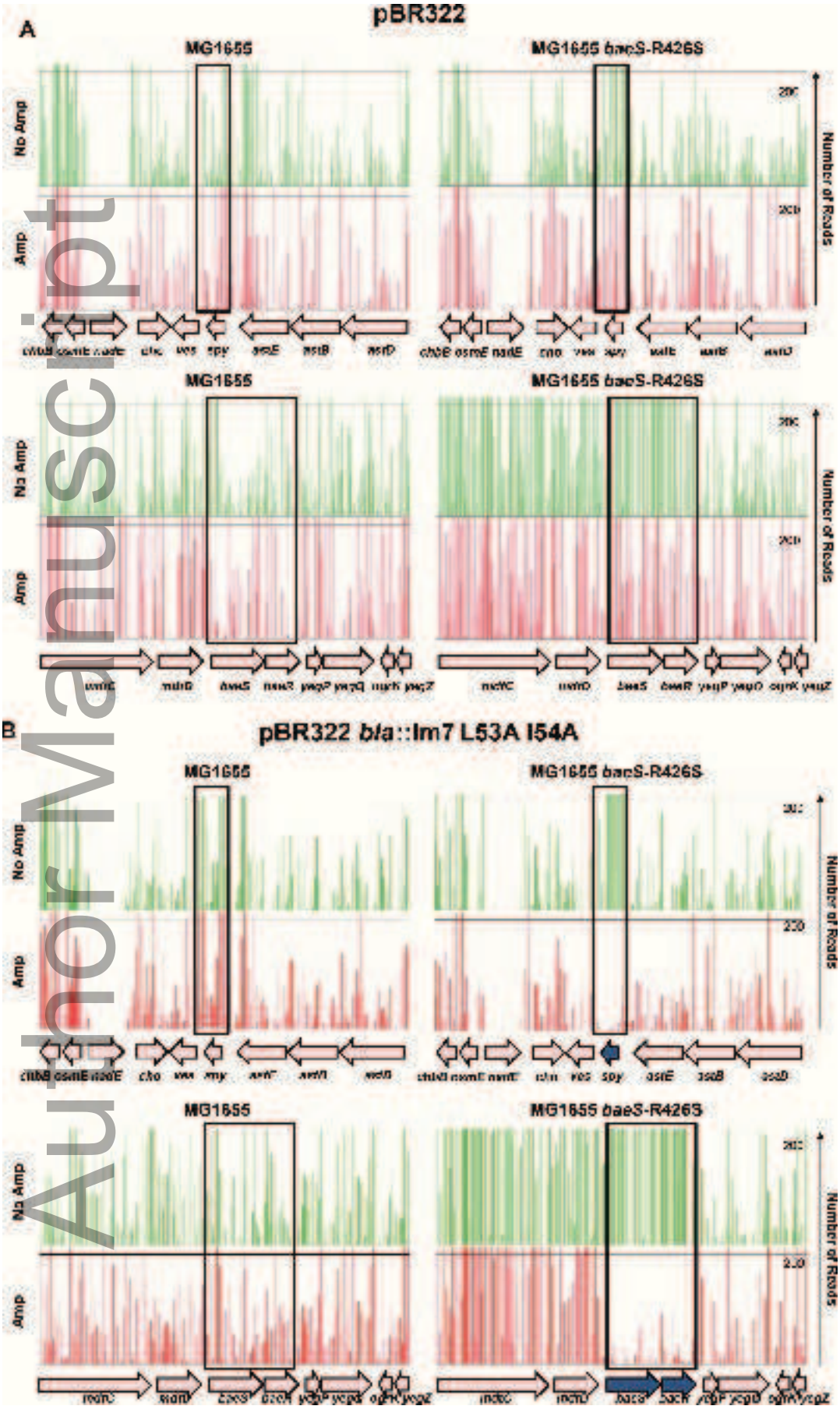

embj_2019104231_f1ev.tif

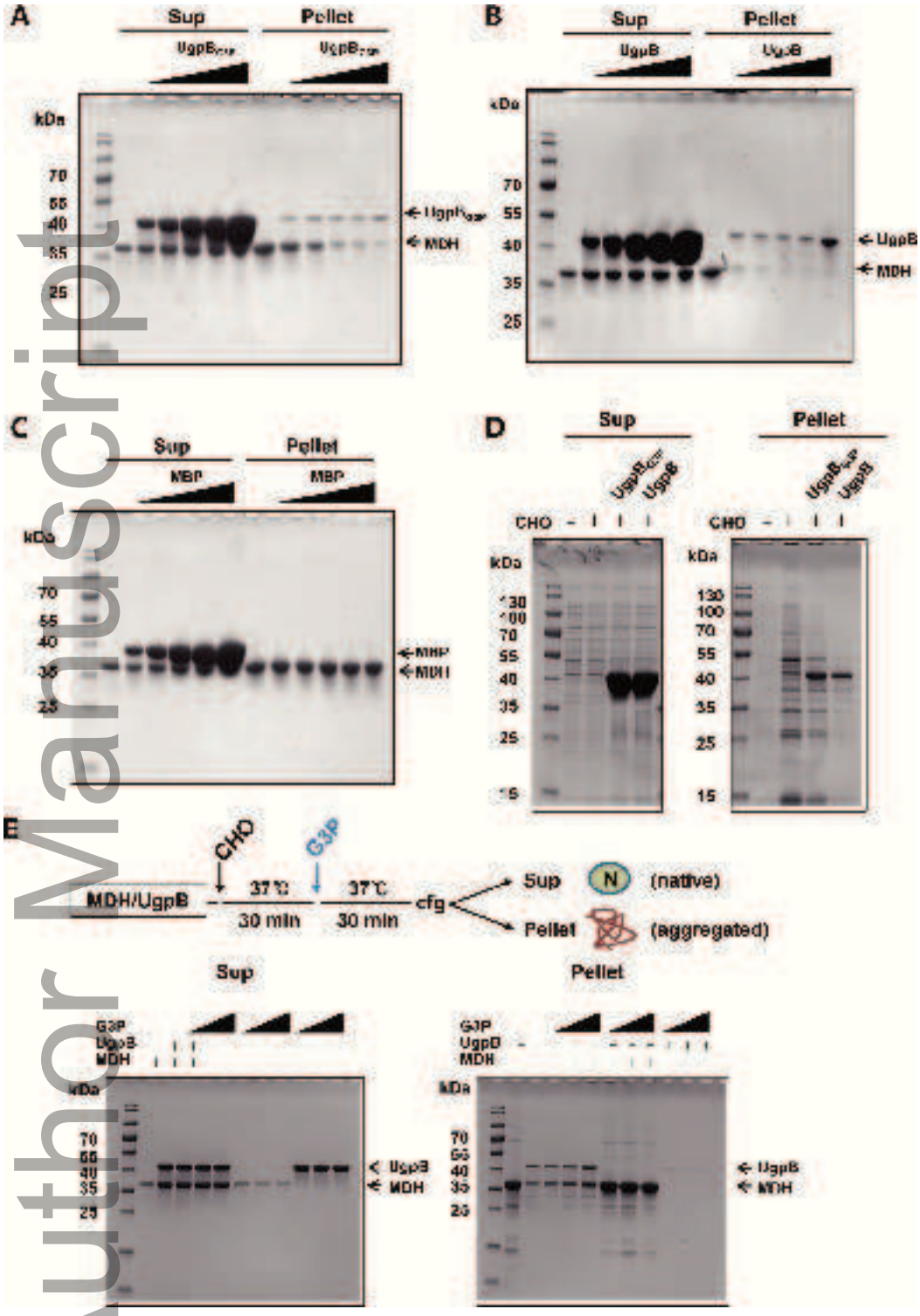

embj_2019104231_f2ev.tif

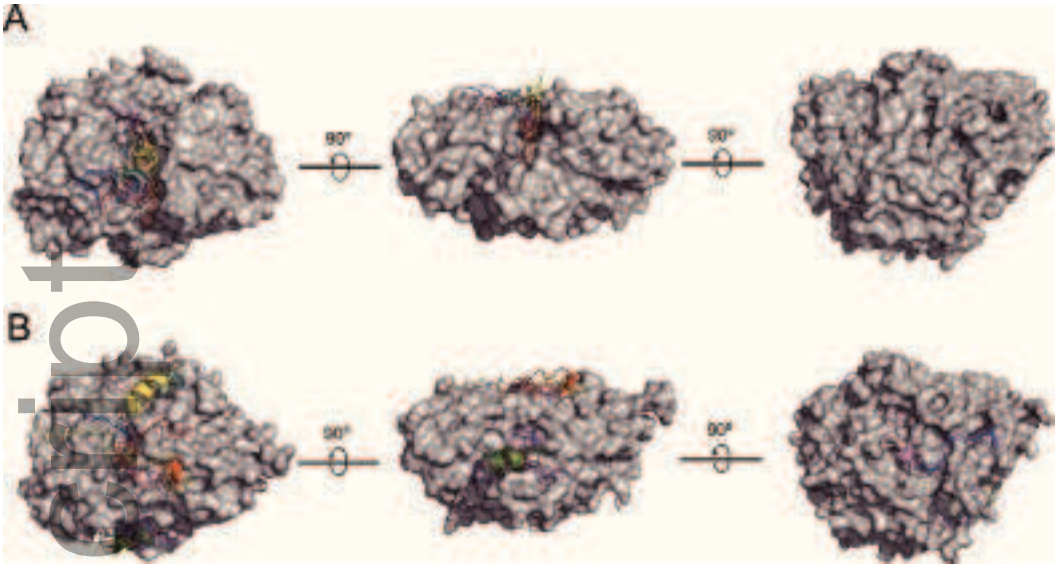

embj_2019104231_f3ev.tif

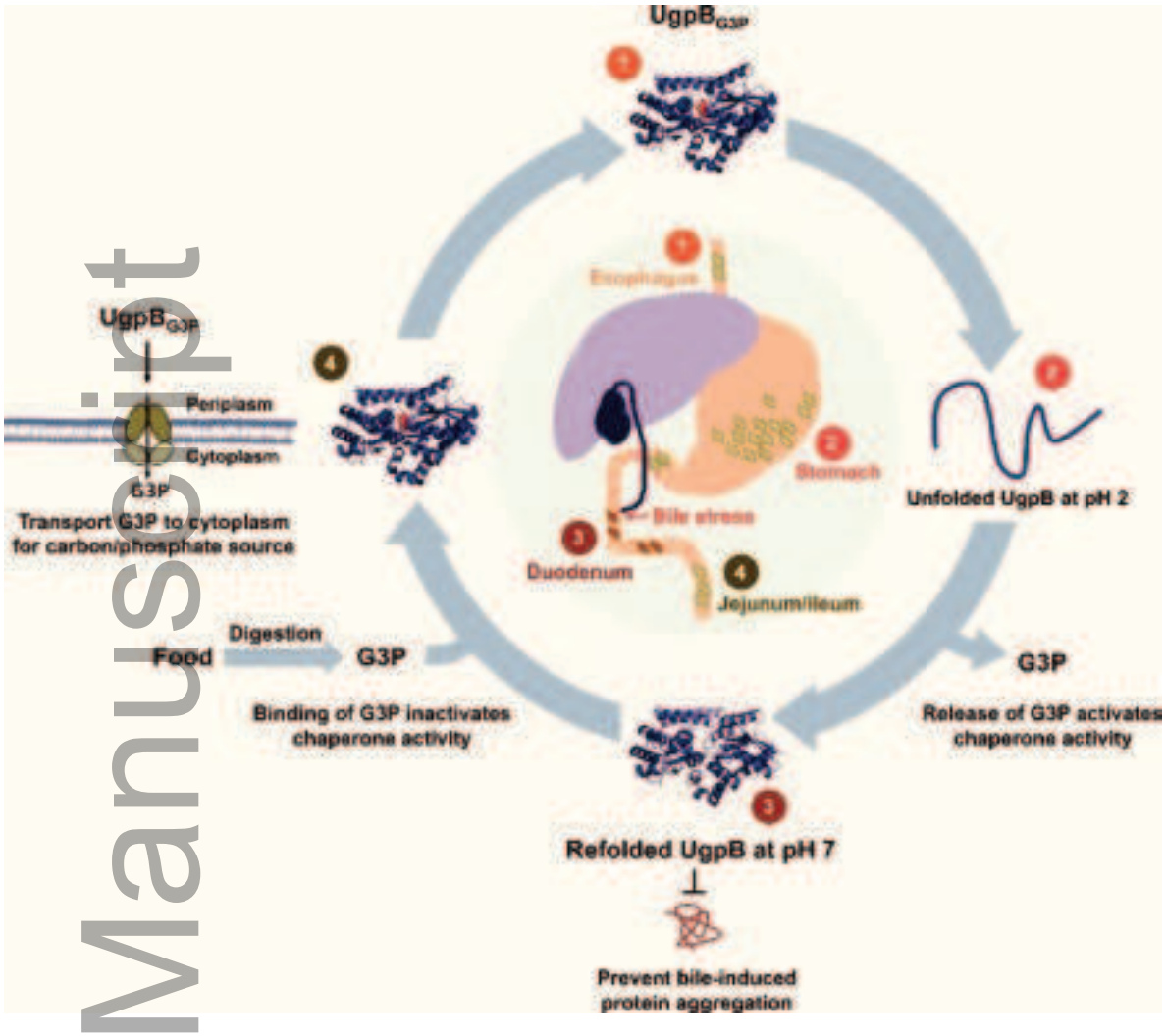

embj_2019104231_f4ev.tif

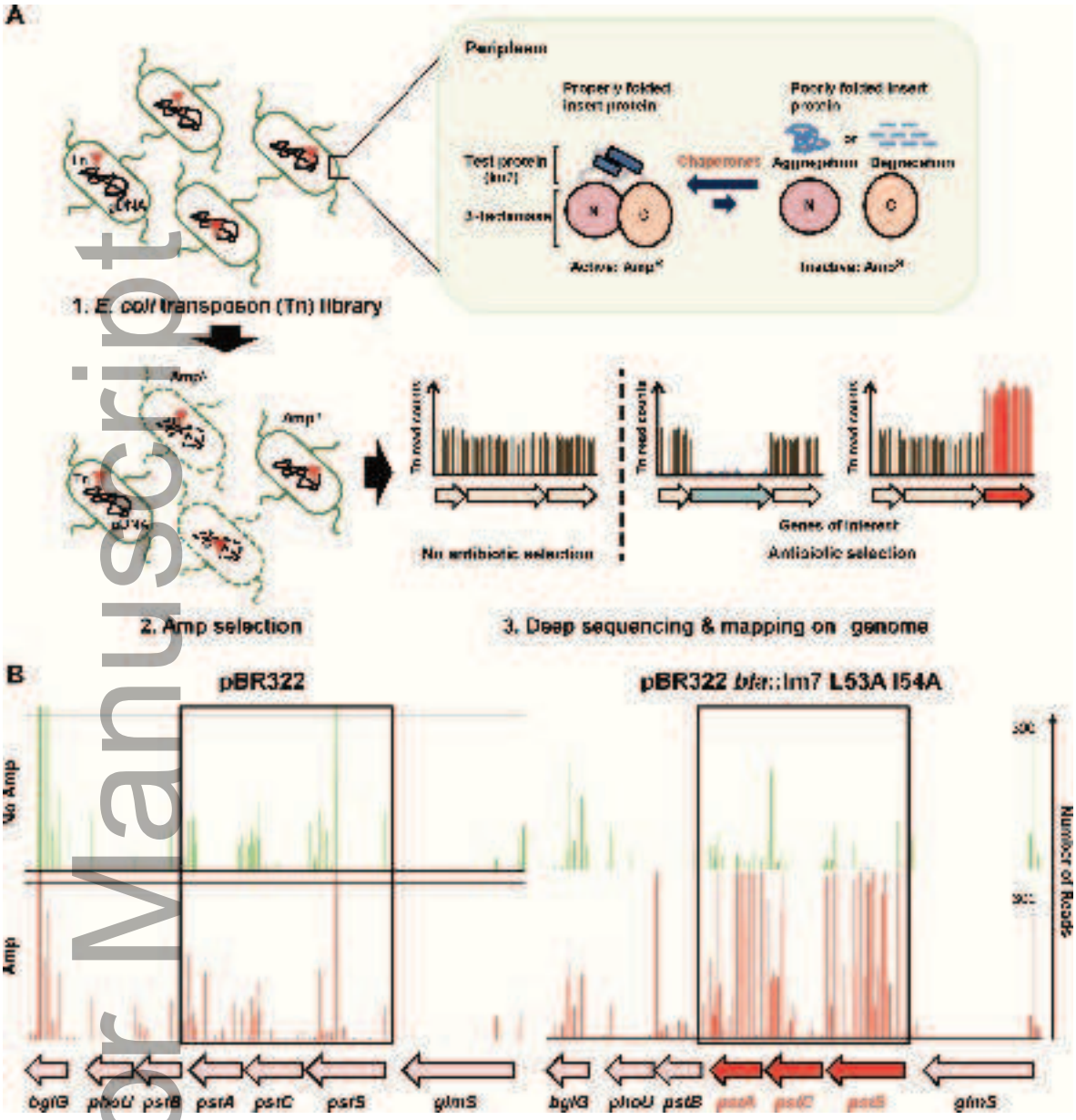

embj_2019104231_f1.tif

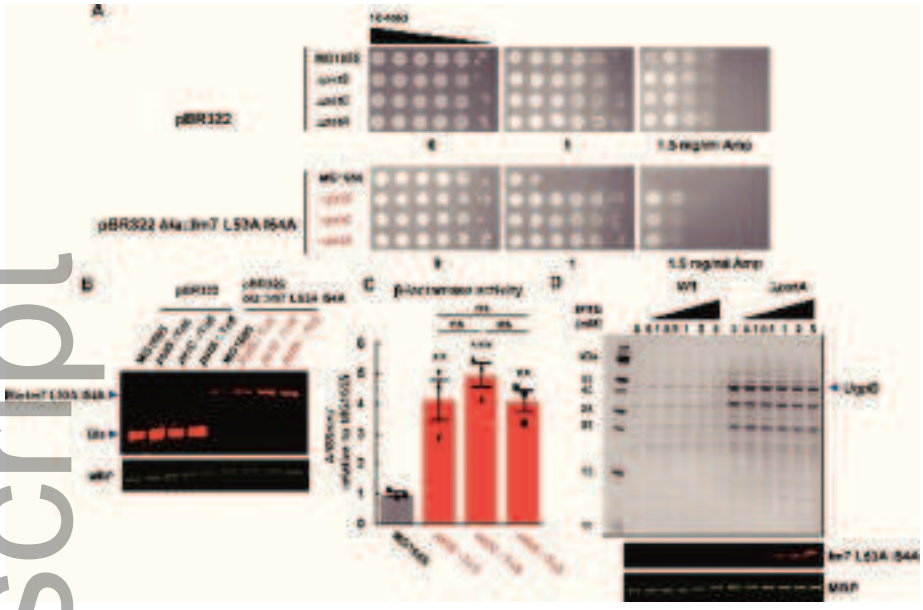

embj_2019104231_f2.tif

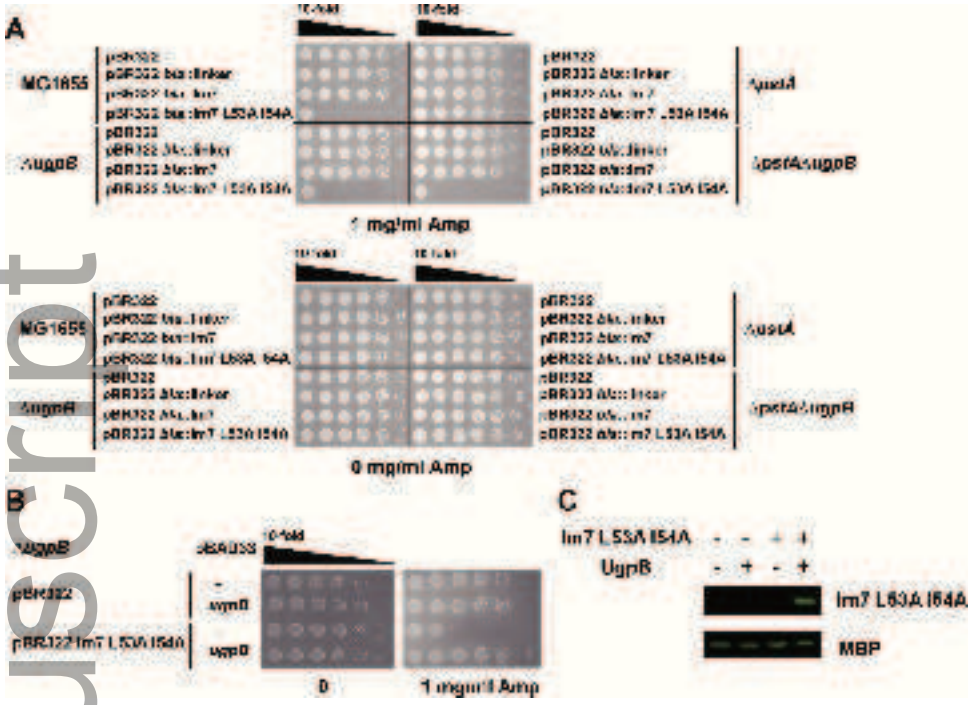

embj_2019104231_f3.tif

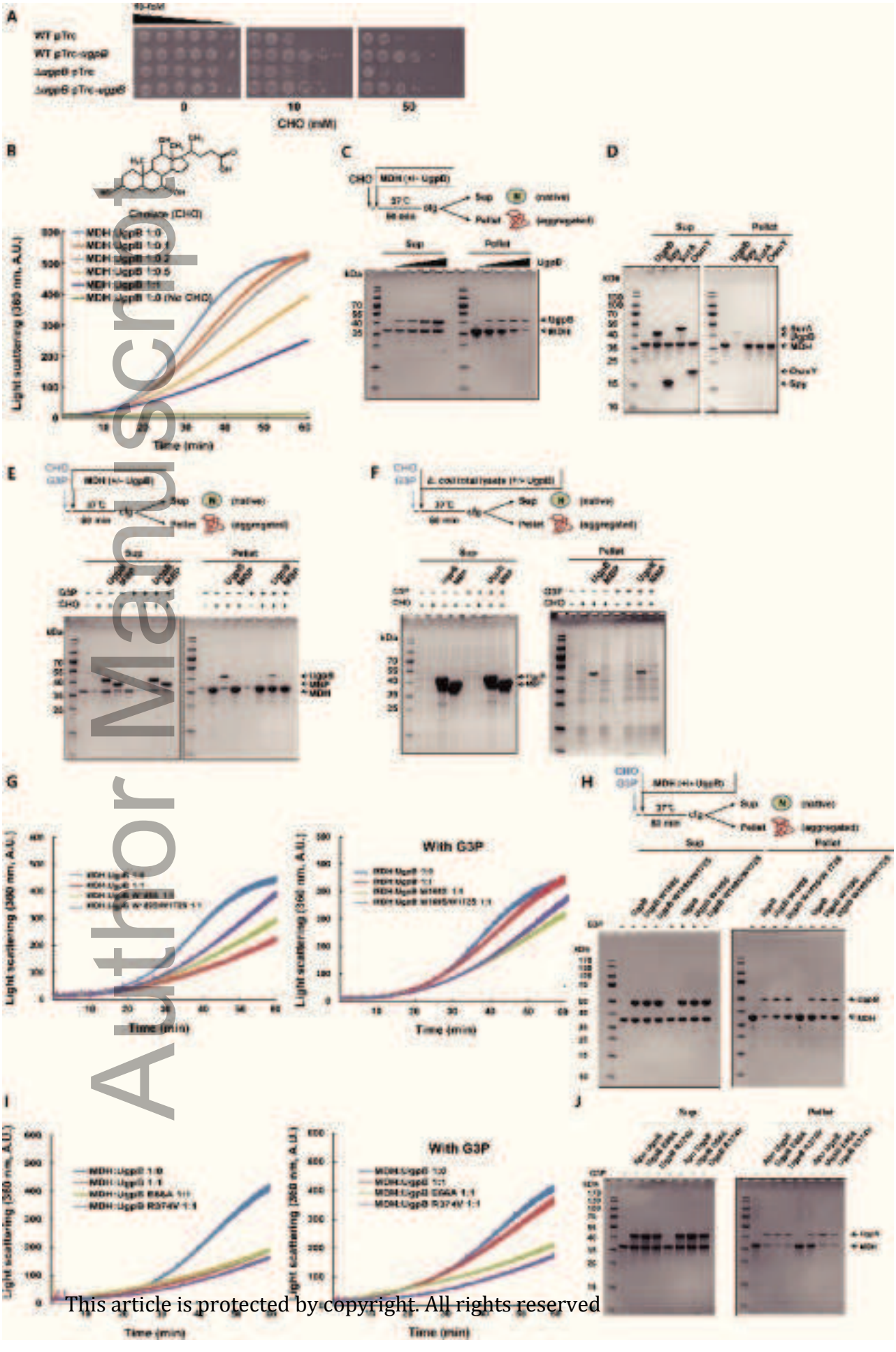

embj_2019104231_f4.tif

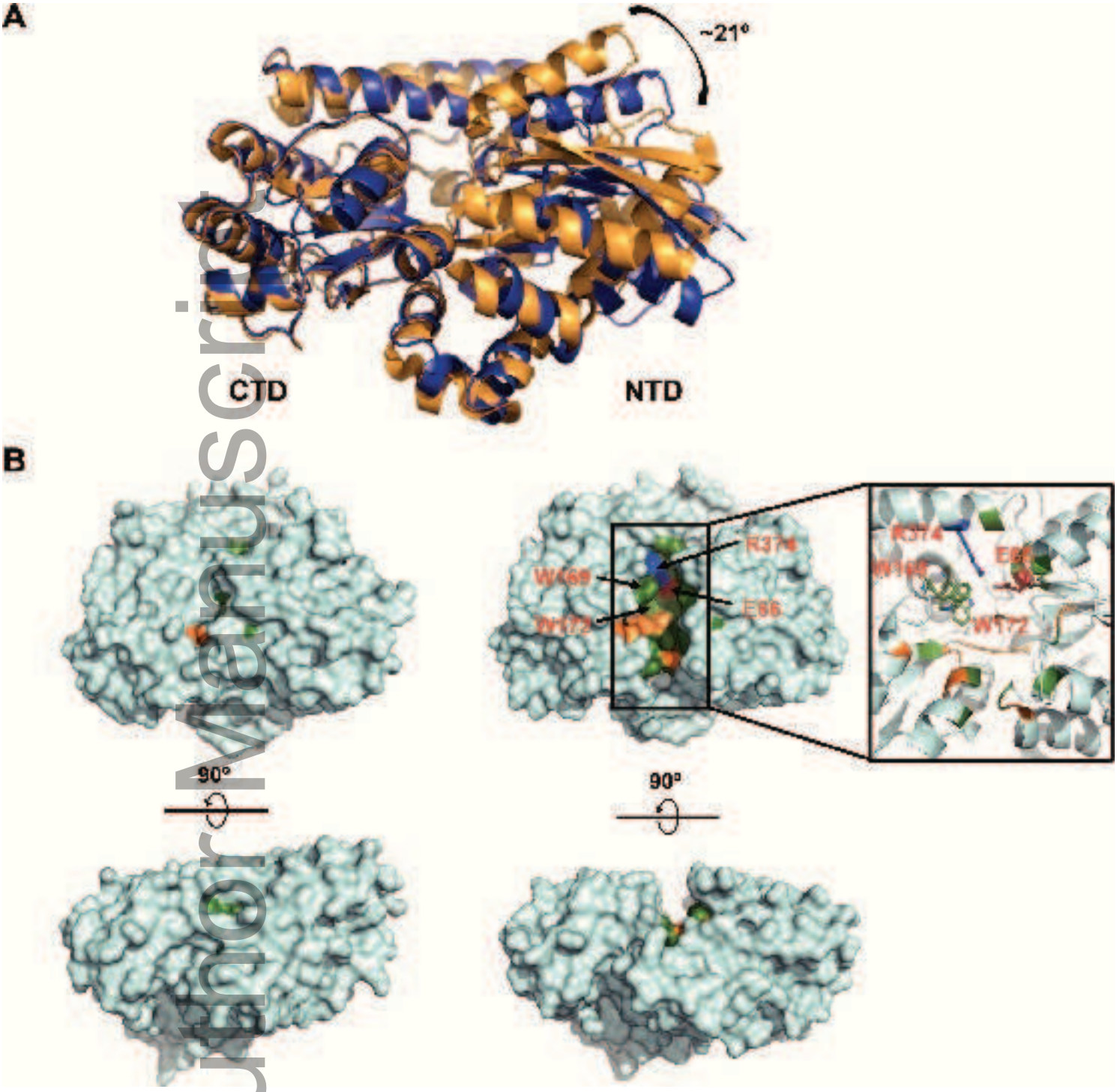

embj_2019104231_f5.tif

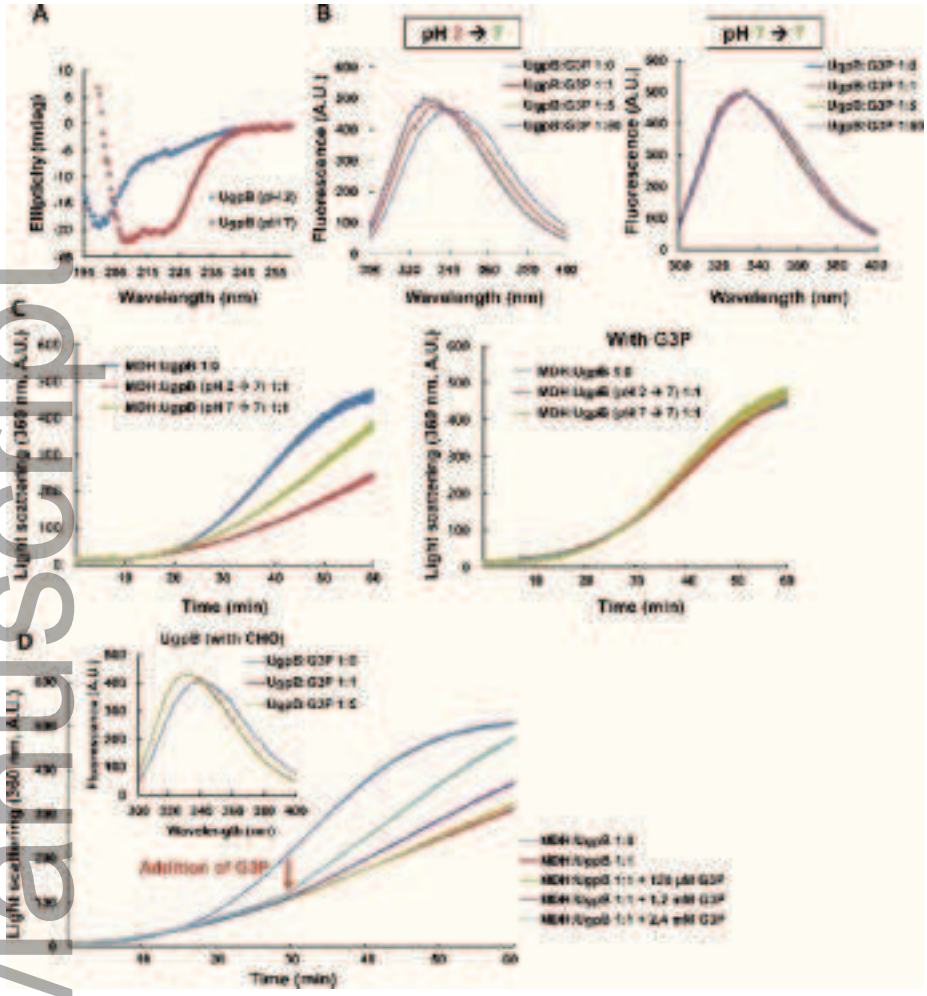

embj_2019104231_f6.tif